Li-rich pegmatites and related peraluminous granites of the Fregeneda-Almendra field (Spain-Portugal): A case study of magmatic signature for Li enrichment

Encarnación Roda-Robles [a,*], Romeu Vieira [b], Alexandre Lima [b,c], Jon Errandonea-Martin [a], Alfonso Pesquera [a], Joana Cardoso-Fernandes [b,c], Idoia Garate-Olave [a]

[a] Department of Geology, Basque Country University (UPV/EHU), Barrio Sarriena s/n, 48940 Leioa, Spain
[b] Institute of Earth Sciences (Porto Pole), University of Porto, Rua do Campo Alegre, 687, 4169-007 Porto, Portugal
[c] DGAOT, Faculty of Sciences, University of Porto, Rua do Campo Alegre, 687, 4169-007 Porto, Portugal

ABSTRACT

Based on field and petrographic observations, mineralogical, geochemical (whole-rock by ICP-MS, ICP-OES, ISE and PGNAA) and geochronological (Ar—Ar on mica and U—Pb on columbite) data, ten pegmatite types and one type of cassiterite-rich quartz hydrothermal veins have been distinguished in the Fregeneda-Almendra field (FA) (Central Iberian Zone), some of them highly enriched in Li (included in petalite, spodumene and Li-rich mica). The pegmatites and the veins mostly intrude Neoproterozoic to Cambrian rocks from the Schist-Greywacke Complex. Felsic igneous magmatism during *syn*- to late-D$_3$ stages ($\approx$ 320–295 Ma) of the Variscan orogeny was important and nearly continuous in the area, with the overlap of different granitic units of highly per-aluminous S-type composition. The most important in outcrop corresponds to the Mêda-Escalhão-Penedono-Lumbrales granitic complex (MEPL), which belongs to a two-mica leucogranitic series. The other granitic units (Saucelle, Feli and East-MEPL granites) are younger and belong to a P-rich, Ca-poor monzogranitic series. Spatial relationships, together with chemical, mineralogical and geochronological data, indicate that all the pegmatite types and the cassiterite-rich quartz hydrothermal veins are not cogenetic, being related to three different magmatic events: (i) ($\approx$ 319–313 Ma) includes the *syn*-D$_3$ MEPL granite and three types of barren pegmatites (intragranitic, quartz+andalusite layers and simple concordant pegmatites); (ii) ($\approx$ 305–300 Ma) corresponds to the late to post-D$_3$ Feli granite, related to a group of cassiterite-rich quartz veins; and, (iii) ($\approx$ 300–298 Ma) represents the late- to post-D$_3$ East-MEPL and Saucelle granites, likely parental of some barren aplitic-pegmatitic apophyses and the discordant intermediate and Li-rich pegmatites. These latter form part of a general granite-pegmatite fractionation trend.

1. Introduction

Granitic pegmatites are coarse-grained magmatic rocks, but highly variable in grain size, characterized by an anisotropic fabric including graphic intergrowths, layered units, comb structures and often miarolitic cavities. Granitic pegmatites may be grouped into two different families (Černý and Ercit, 2005): (i) LCT (from Li-Cs-Ta) that occur in orogenic belts; and (ii) NYF (from Nb-Y-F), which are mainly anorogenic. LCT are overall more common than NYF pegmatites. These rocks often represent the transition between the magmatic and the

hydrothermal stages, which makes pegmatites witnesses of the important chemical and physical variations that must take place in volatile-rich magmatic systems. Since the early works of Fersman (1940), Cameron et al. (1949) and Jahns (1953), numerous studies have been carried out from different perspectives on pegmatites, all intending to cast light on understanding their origin and significance. However, several aspects concerning the petrogenesis of pegmatites are still not fully understood (e.g. London, 2008, 2018; Simmons and Webber, 2008). One of the most controversial questions is related to the origin of the pegmatitic melts. A magmatic source, with the pegmatitic melts

being formed via fractional crystallization of a parental granitic melt, commonly S-type for the LCT family, has been the most accepted model for decades (e.g., Breiter et al., 2021; Černý, 1992; Garate-Olave et al., 2020; London, 2008; Neiva et al., 2019). In contrast, an anatectic origin for the pegmatitic melts has also been suggested for numerous pegmatites (e.g., Norton, 1973; Novák et al., 2013; Simmons et al., 2016; Simmons and Webber, 2008; Sokolov, 1982; Webber et al., 2019). In this case, authors propose that low proportions of partial melting of a suitable protolith may produce small volumes of melt enriched in incompatible elements, which is the typical signature of the most fractionated pegmatitic bodies.

In recent years the growing economic interest in pegmatites has prompted numerous exploration campaigns along different pegmatite belts worldwide. The Central Iberian Zone (CIZ) is being intensively explored for Li and also for Ta and Sn. It encloses several Li-rich pegmatitic fields (at least 12) with some tens to hundreds of pegmatitic bodies (Roda-Robles et al., 2016, 2018 and references therein). In many of those fields, pegmatitic dykes with variable degree of fractionation are present, from barren to highly-evolved Li-rich pegmatites. The Fregeneda-Almendra pegmatitic field (FA) is one of the most complex fields occurring in the region. There, 10 different types of pegmatites have been distinguished, four of them containing Li, which is mainly hosted in spodumene, petalite and Li-mica (e.g., Roda-Robles, 1993; Vieira, 2010). They are contemporaneous with protracted peraluminous granitic magmatism during synkinematic to late and post-Variscan stages. This study builds upon previous works (e.g., Roda et al., 1995a, 1995b, 1996; Roda-Robles, 1993; Roda-Robles et al., 1999, 2009, 2010; Vieira, 2010; Vieira et al., 2011), which have mainly focused on the petrography and detailed mineralogy of the different pegmatite types. However, a petrogenetic model of the whole pegmatitic field, discussing the origin (magmatic or anatectic) and evolution of the

pegmatitic melts; the structural facts; as well as the relationships between the granites and pegmatites and among the different pegmatite types, has not yet been proposed. In this work, we integrate exhaustive field observations, petrographic and mineralogical data, whole-rock geochemistry, together with geochronological and structural data, in order to shed light on the processes involved in the genesis of the different pegmatites from the Fregeneda-Almendra area and their sources.

2. Regional geology

2.1. Structure and metamorphism

The FA area forms part of a narrow strip of pre-Ordovician metamorphic terrains where the lowest group belongs to the Schist-Greywacke Complex (SGC). This complex consists of a very thick psammopelitic sequence of Neoproterozoic to lower Ordovician age with minor intercalations of quartzites, conglomerates, amphibolites, calc-silicate and volcaniclastic layers (Talavera et al., 2012 and references therein) (Figs. 1, 2).

The FA area shows the effects of Variscan polyphasic deformation and metamorphism (e.g., Díez Fernández and Pereira, 2016). The initial deformation phase (D_1) related to crustal thickening yielded WNW–ESE striking folds with an associated S_1 schistosity (Rodríguez Fernández et al., 2000; Silva and Ribeiro, 1994). During D_1 low-grade Barrovian-type metamorphism with peak conditions in the greenschist facies affected the entire belt (chlorite and biotite zones in metapelites; Díez Fernández and Pereira, 2016; Dias da Silva et al., 2017). In the nearby Tormes Dome the first metamorphic event peaked at 337–332 Ma (e.g., López-Moro et al., 2018 and references therein). The second deformation phase (D_2) took place between 330 and 320 Ma and was
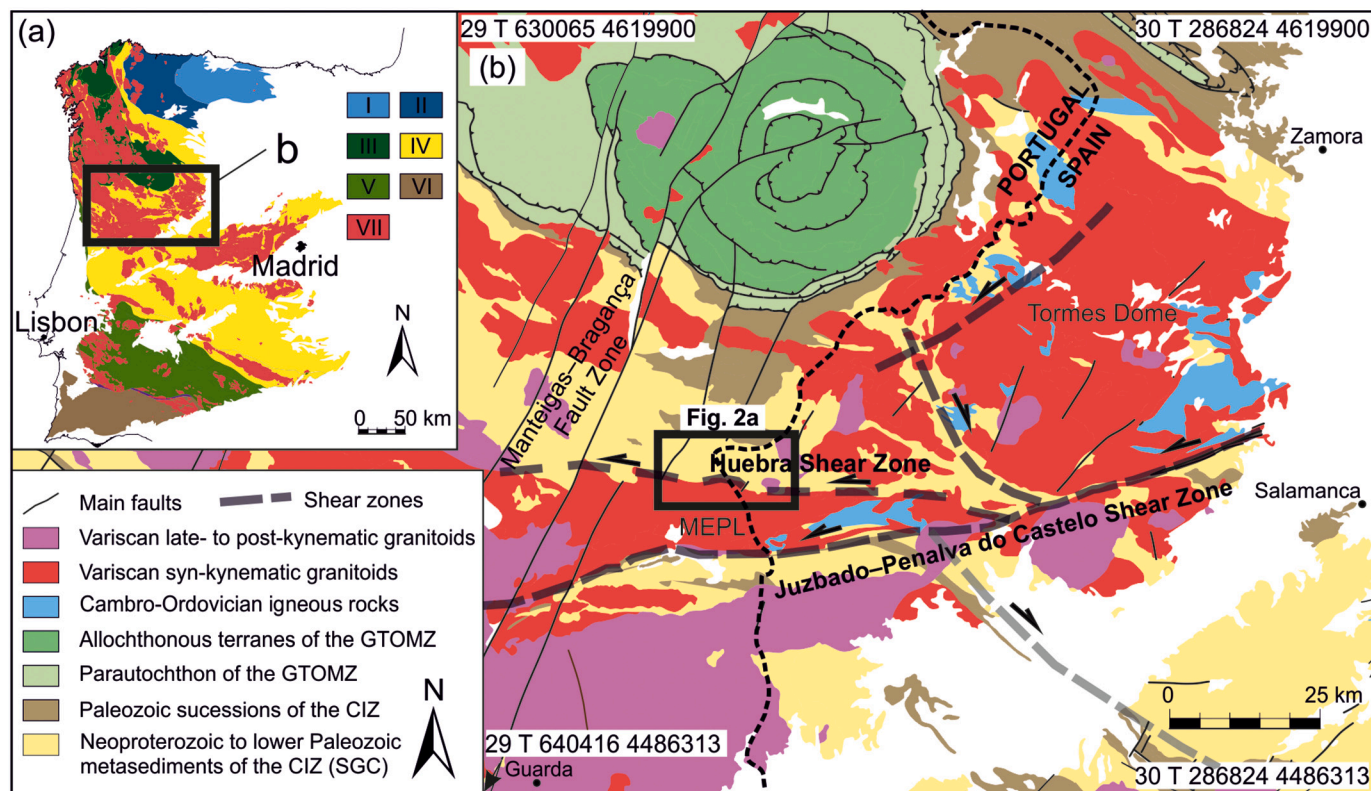

Fig. 1. (a) Geological map of the Iberian Massif, subdivision based on Julivert et al. (1972) and Variscan granitoids adapted from Rodríguez Fernández and Oliveira (2015). I: Cantabrian Zone, II: West Asturian-Leonese Zone, III: Galicia-Trás-os-Montes Zone (GTOMZ), IV: Central Iberian Zone (CIZ), V: Ossa-Morena Zone, VI: South Portuguese Zone, VII: Variscan granitoids; (b) Regional geological map modified from Errandonea-Martin et al. (2022). Shear zones from Díez Fernández and Pereira, 2016. MEPL = Mêda-Escalhão-Penedono-Lumbrales granitic complex. SGC = Schist-Graywacke Complex.
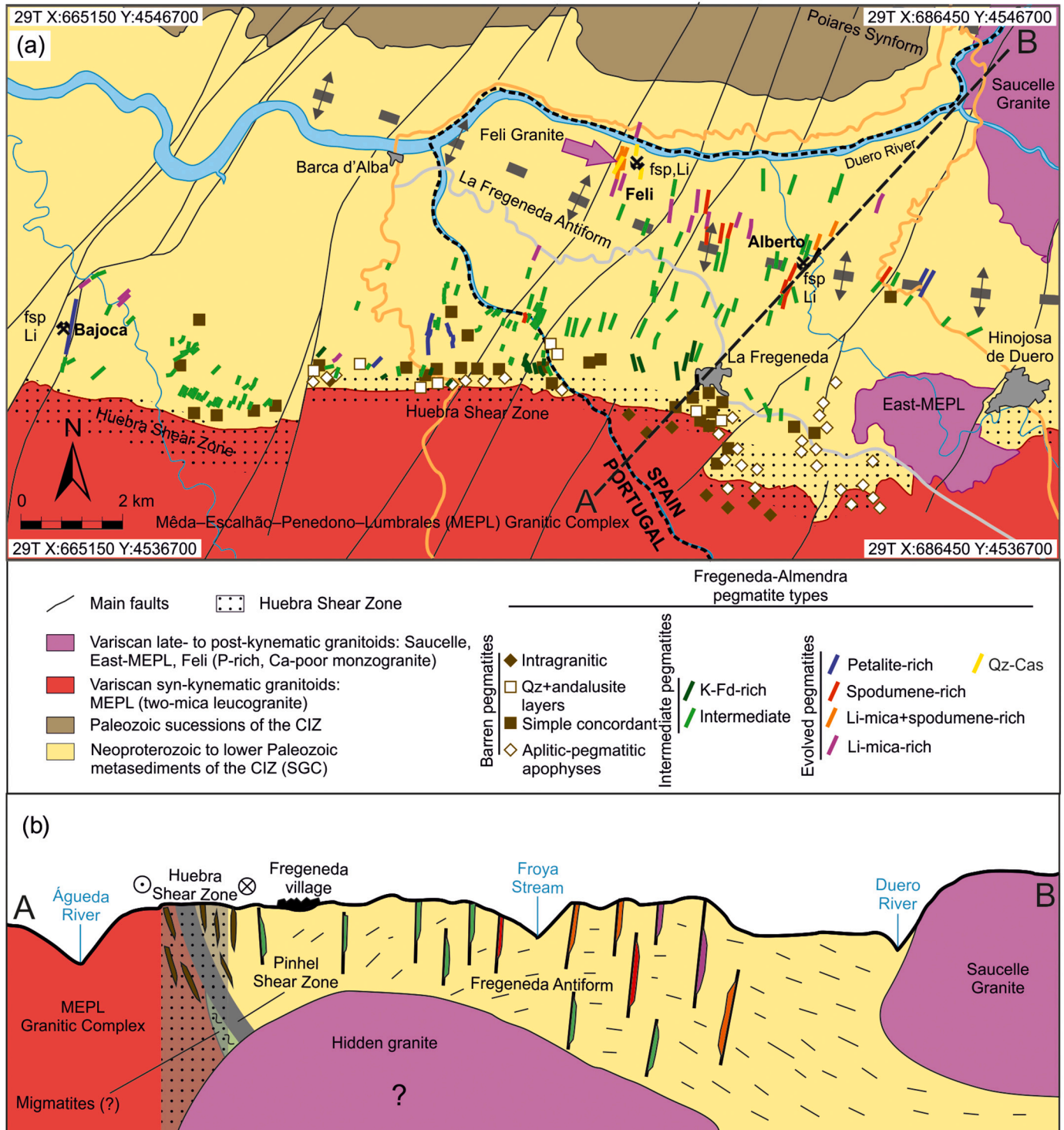
Fig. 2. (a) Schematic geological map of the Fregeneda-Almendra area, modified after Silva and Ribeiro (1994), Rodríguez Fernández et al. (2000) and Vieira et al. (2011); (b) cross-section (A-B) of the FA field.

responsible for the exhumation of anatectic domes and high-temperature low-pressure metamorphism (Dias da Silva et al., 2017; Díez Fernández and Pereira, 2016, 2017; López-Moro et al., 2018). The limit between the main low-grade metamorphic area and high-grade rocks such as gneisses and migmatites occurs along a tectonic contact in the SW of the FA field. This supports the exhumation of these high-grade rocks may have occurred through the Pinhel Shear Zone (Fig. 2b), whose maximum activity has been defined in the range of 321–317 Ma (e.g., Díez Fernández and Pereira, 2016; Pereira et al.,

2018). Deformation associated with the third phase (D₃), developed during retrograde metamorphism, between 320 and 305 Ma, gave rise to first-order ductile transcurrent sub-vertical shear-zones with associated S₃ foliation (Dias da Silva et al., 2017; Díez Fernández and Pereira, 2017). The timing of D₃ has been constrained to 317–307 Ma, with the Huebra Shear Zone (HSZ) marking in some areas the current limit between the low-grade and high-grade rocks in FA (Díez Fernández and Pereira, 2017 and references therein) (Figs. 1, 2). Later D₄ structures in the area comprise the large-scale Juzbado-Penalva do Castelo Shear

Zone (JPSZ) (Fig. 1), which has been dated from synkinematic muscovite $^{40}Ar/^{39}Ar$ data and U—Pb zircon geochronology yielding ages of ca. 309–305 Ma (Díez Fernández and Pereira, 2017; Gutiérrez-Alonso et al., 2015). The JPSZ is considered later than the HSZ, but a reactivation of the HSZ during subsequent sinistral deformation associated with the JPSZ is possible (Díez Fernández and Pereira, 2017). All these structures in FA are cut by NE–SW to NNE–SSW faults (Rodríguez Fernández et al., 2000; Silva and Ribeiro, 1994).

2.2. Variscan granitic magmatism

The CIZ is characterized by a large volume of granitic rocks linked to the Variscan orogeny, with crust-derived peraluminous granitic rocks predominant over metaluminous granitic and basic rocks (Villaseca et al., 1998a). Three granite groups have been distinguished relative to Variscan D3 deformation: pre-, *syn*- and late- to post-kynematic (Dias et al., 1998; López-Plaza and Martínez-Catalán, 1987). In addition, these granites have been subdivided into five different suites on the basis of petrographic and geochemical characteristics (Roda-Robles et al., 2018; Villaseca, 2011): (1) two-mica leucogranites, highly peraluminous, Ca-poor and variably enriched in P, with a metasedimentary source (mostly emplaced during D3: 320 ± 6 Ma, on average) (e.g., Gomes et al., 2014; López-Moro et al., 2012); (2) P-rich, Ca-poor, highly peraluminous biotite ± muscovite ± cordierite ± andalusite monzogranites. Most intrusions are zoned allochthonous plutons emplaced at shallow crustal levels ($\approx$ 2–3 kbar) and are younger ($\approx$ 310-300 Ma) than the two-mica leucogranites (e.g., Errandonea-Martin et al., 2019; González-Menéndez et al., 2011). As for the two-mica leucogranites, a mainly metasedimentary source is attributed for the P-rich, Ca-poor monzogranites; (3) P-poor moderately peraluminous granites, mostly crystallized at 308–299 Ma; (4) moderately to low peraluminous granites, with features at the limit between S- and I-type granites, with emplacement ages of 319–299 Ma; and (5) I-type granites including metaluminous to low peraluminous amphibole-bearing biotite-granodiorites (see Roda-Robles et al., 2018 for a more detailed characterization of these suites).

The FA pegmatitic field is confined to the south by the syn-D3 Mêda-Escalhão-Penedono-Lumbrales granitic complex (MEPL) (e.g., Ferreira et al., 2019; Rodríguez Fernández et al., 2000), which belongs to the two-mica leucogranites suite of Roda-Robles et al. (2018); whereas to the NE the FA field is confined by the late- to post-D3 Saucelle granite, which belongs to the P-rich, Ca-poor monzogranites suite (Fig. 2). In addition to these two outcropping granites, exploration drills executed in the Feli open pit, located in the north of the FA field, detected a hidden granitic cupola (Feli granite) (Fig. 2) (Mangas and Arribas, 1988; Martín-Izard et al., 1992; Vieira, 2010).

2.2.1. Mêda-Escalhão-Penedono-Lumbrales granitic complex (MEPL)

The MEPL granitic complex is bordered by two strike-slip EW to ENE-WSW trending sinistral shear zones: the D3 Huebra shear zone (HSZ) to the north and the D4 Juzbado-Penalva do Castelo shear zone (JPSZ) to the south (Díez Fernández and Pereira, 2016, 2017; Ferreira et al., 2019, 2020) (Figs. 1, 2). The exhumation of high-grade rocks of the MEPL, developed most probably via extensional shear zones such as the Pinhel Shear Zone (Fig. 2b), started during D2, whereas the HSZ and JPSZ shear zones would be involved in the final emplacement of the MEPL granites during D3 (Díez Fernández and Pereira, 2016; Pereira et al., 2017).

The MEPL includes different peraluminous granitic facies and a migmatitic unit (Ferreira et al., 2019, 2020). Most of the granitic facies are coeval with the third deformation phase in the area (D3) (Ferreira et al., 2019; Pereira et al., 2018), whereas a minor, non-foliated granitic facies that intrudes discordantly D3 structures has been also described to the south (Díez Fernández and Pereira, 2017). Another non-deformed granitic intrusion has been observed in the east of the MEPL, within the FA area, named as East-MEPL (Figs. 1, 2) (Gonzalo Corral, 1981).

2.2.2. Saucelle granite

The Saucelle granite is a late- to post-D3 and highly peraluminous two-mica leucogranite that crops out in the NE of the FA area (Fig. 2). The most representative facies corresponds to a medium-grained two-mica leucogranite, whereas in its SW border a marginal, finer-grained, muscovite-rich facies is found. This undeformed granite intrudes north to the Fregeneda antiform and cuts a D3 minor shear zone subsidiary to the HSZ (Dias da Silva, 2014; Silva and Ribeiro, 1994). It is strongly fractured following a N10°-30°E strike, parallel to the Duero River canyon, as a result of the brittle late-Variscan and Alpine deformations (Dias da Silva, 2014).

2.2.3. Feli granite

Various authors indicate the existence of a hidden granite intrusion in the FA area (Mangas and Arribas, 1988; Martín-Izard et al., 1992; Vieira, 2010), which was detected by exploration drills made in the northern part of the FA field, in the Feli open pit (Fig. 2a). The Feli pluton is a two-mica (Ms > > Bt) leucogranite, fine- to medium-grained, chemically quite similar to the main facies of the Saucelle granite (Vieira, 2010). Evidence for metasomatic overprint is provided by the replacement of most of the biotite by zinnwaldite and/or tourmaline (schorl).

2.2.4. Pre-existing geochronological data of the igneous rocks from the FA area

Some granitic rocks of the FA have already been the subject of geochronological dating. For example, García Garzón and Locutura, (1981) presented ages of 300 ± 8 Ma (Rb—Sr) for the Lumbrales–Sobradillo granite (Spanish sector of the MEPL granitic complex). Recently, Pereira et al. (2018) obtained an age of 318.7 ± 4.8 Ma (LA-ICP-MS U—Pb in zircon) for the Mêda-Escalhão-Penedono massif, which is the western sector of the MEPL; and Ferreira et al. (2019) dated five different facies also from the west side of the MEPL (U—Pb in zircon), with ages clustering around 317-313 Ma for four *syn*-tectonic facies, and an age of 300 ± 2 Ma for a late-tectonic granite.

In the case of the pegmatites, the Li-mica-rich Riba D'Alva body, located north of the Feli mine, was dated giving an age of 292 ± 3 Ma (Rb-Sr; Nitschke, 1999). The same work presents values of 298 ± 1 Ma and 297 ± 1 Ma ($^{40}Ar*/^{39}Ar$) for a Sn-W-mineralized stockwork, 1.5 km NW of the Riba D'Alva mine.

3. Geology of the FA pegmatites

Most pegmatites from the FA field are hosted by metasedimentary rocks of the SGC except a few intragranitic occurrences. Based mainly on field relationships, mineralogical and geochemical data, as well as on structural and textural features, 10 types of pegmatites have been distinguished. In addition, some Sn-rich quartz veins occur in the north of the field (Roda-Robles, 1993; Roda-Robles et al., 1999; Vieira, 2010; Vieira et al., 2011) (Fig. 2, Table 1). Most pegmatites are poorly evolved, but $\approx$ 10% of the pegmatitic bodies of the FA correspond to fractionated pegmatites, with Li-minerals (Roda et al., 1995a, 1995b; Roda-Robles et al., 1999; Vieira, 2010).

3.1. Barren pegmatites

Four types of barren pegmatites have been recognized in the FA (Table 1, Fig. 2). (1) *Intragranitic pegmatites* that are relatively abundant in the northern MEPL border. They occur as thin (< 30 cm thick), elongated bodies (up to $\approx$ 3 m long) (Fig. 3a), striking around N030°-050°E along the granite fractures and dipping sub-vertically. The mineral assemblages are dominated by K-feldspar, muscovite, albite and tourmaline, with minor biotite and accessory phosphates. Usually, these pegmatites show a well-developed internal structure, with a prominent quartz core. (2) *Quartz + andalusite layers* that are hosted by metasedimentary rocks near the contact with the MEPL granite (Fig. 2). They are

Table 1
Main characteristics of the pegmatite types and hydrothermal veins recognized in the Fregeneda-Almendra area.

PEGMATITE GROUP	PEGMATITE TYPE	MINERALOGY		RELATION TO HOST-ROCK & STRUCTURE	REMARKS	ENRICHMENTS	RELATION TO DEFORMATION	AGE RANGE (magmatic event*)
		Main	Minor					
BARREN PEGMATITES	Intragranitic pegmatites	Qz, Kfs	ms, ab, tur	- N030-050E	Intragranitic (MEPL) dyke-like, < 30 cm thick	scarce, intragranitic	K, Al, (B, P)	affected by D$_3$	311–319 Ma (1)
	Quartz + andalusite layers	Qz, and	ms, tur, Kfs	Concordant N100-120E	SGC metasediments, dyke-like, < 50 cm thick	scarce, boudinage structures	Al, Si, (B, K)	affected by D3 and HSZ	311–319 Ma (1)
	Simple concordant pegmatites	Qz, Kfs, ab, ms, tur	and, chl, grt, bt, ap	Concordant N100-120E	SGC metasediments, dyke-like, < 2 m thick	common, graphic texture, locally with internal zoning	Al, Na, B	affected by D3 and HSZ	311–319 Ma (1)
	Aplitic-pegmatitic apophyses	Qz, Kfs, ms	ab, tur, bt	Discordant -	SGC metasediments, variable sizes, irregular masses	abundant to the East, aplitic-pegmatitic facies, graphic texture	K, Al, (B, P)	not affected by HSZ	295–300 Ma (3)
INTERMEDIATE PEGMATITES	K-feldspar-rich pegmatites	Kfs	Qz, ms, py	Discordant NS-N030E	SGC metasediments, subvertical dykes, 1–3 m thick	scarce main component is pinkish Kfs	K	not affected by HSZ	295–300 Ma (3)
	Intermediate pegmatites	Qz, Kfs, Ab, ms	Fe-Mn-pho, tur, mbs, CT	Discordant N010-030E	SGC metasediments, subvertical dykes, 10 cm-2 m thick	most abundant, often layering parallel to contacts	Na, K, Al, (P, Li)	not affected by HSZ	295–300 Ma (3)
EVOLVED PEGMATITES	Petalite-rich pegmatites	Qz, ab, pet	ms, mbs, cst, CT	Discordant NS-N030E	SGC metasediments, subvertical dykes, 1–30 m thick	not abundant, no internal zoning. Main body: Bajoca	Li, P, (Sn)	not affected by HSZ	295–300 Ma (3)
	Spodumene-rich	Qz, ab, spd, Kfs	ms, pet, mbs, cst, CT	Discordant NS-N030E	SGC metasediments, subvertical dykes, 4–10 m thick	not abundant, no internal zoning. Main body: Alberto open-pit	Li, P, (Sn)	not affected by HSZ	295–300 Ma (3)
	Li-mica + spodumene-rich pegmatites	Qz, ab, Kfs, Li-mica, spd, ms	mbs, cst, CT, brl, tpz	Discordant NS-N030E	SGC metasediments, subvertical dykes, <15 m thick	scarce, internal layering common Main body: Feli open-pit	Li, Sn, P, F, (Rb, Cs)	not affected by HSZ	295–300 Ma (3)
	Li-mica-rich pegmatites	Qz, ab, Li-mica, Kfs	ms, cst, CT, mbs, tpz	Discordant N010-N040E	SGC metasediments, subvertical dykes, <3 m thick	internal layering common,	Li, Sn, P, F, (Rb, Cs)	not affected by HSZ	295–300 Ma (3)
HYDROTHERMAL VEINS	Qz + cassiterite veins	Qz, cst, ms	ab, Kfs, ap, CT	Discordant	SGC metasediments, folded veins, <50 cm thick	scarce, internal zoning, folded, cross-cut by a Li-rich pegmatite dyke	Sn, Si, K, (P)	not affected by HSZ	300–305 Ma (2)

Qz-quartz; Kfs-K-feldspar; ms-muscovite; ab-albite; tur-tourmaline; and-andalusite; bt-biotite; grt-garnet; py-pyrite; pho-phosphates; mbs-montebrasite; pet-petalite; spd-spodumene; cst-cassiterite; ap-apatite; brl-beryl; ecr-eucryptite; CT-columbite-tantalite group minerals; tpz-topaz. *See text (Discussion chapter) and Fig. 11 for explanation on the magmatic events. SGC = Schist-Greywacke Complex. HSZ = Huebra Shear Zone.

unzoned bodies and concordant to the host-rocks along the S$_3$ foliation (N100°-120°E), with variable dip and thickness < 50 cm, commonly showing strong boudinage (Fig. 3b). Andalusite and quartz are the main minerals, with minor K-feldspar, muscovite, schorl, garnet and chlorite. The metasedimentary rocks may be strongly tourmalinized along the contact with these layers. (3) *Simple concordant pegmatites* that are parallel to the S$_3$ foliation (N100°-120°E) (Fig. 3c). These dykes are parallel to the MEPL contact and show a gradual transition to it. They show mylonitization and boudinage. The mineral assemblage is largely dominated by quartz, K-feldspar, muscovite and albite, with minor tourmaline, andalusite, chlorite, garnet, biotite and apatite. In some dykes it is possible to observe an internal zonation. Tourmalinization also occurs along the contact zone with metasedimentary rocks. (4) *Aplitic-pegmatitic apophyses* that are unzoned with variable sizes (< 6 m^2 up to 1km^2 in outcrop) and shapes, from irregular and bulbous masses to ellipsoidal, lens-like, or turnip-shaped forms (Fig. 3d) (Roda-Robles et al., 1999). These bodies outcrop nearby the MEPL granite contact,

being particularly abundant in the east of the field, in close relation to the East-MEPL undeformed granitic unit (Fig. 2). Quartz, K-feldspar, plagioclase and muscovite are the major components of the rocks, with minor biotite, tourmaline and Fe—Mn phosphates.

3.2. Intermediate pegmatites

In general these pegmatites are located further to the north of the MEPL than the barren bodies (Fig. 2), and are subvertical dykes clearly discordant to the regional foliation. They show notable paragenetic and chemical differences relative to the barren pegmatites, with the occurrence of F- and Li-bearing minerals, such as montebrasite, and Nb-Ta-Sn oxides as common accessory phases (Table 1). Two types can be distinguished. (1) *K-feldspar-rich pegmatites*, which are quite scarce, outcropping ≈ 1 km to the north contact of the MEPL granite (Fig. 2). They are subvertical dykes, clearly discordant to the regional foliation with strikes between NS and N030°E. The orange tonality of these dykes
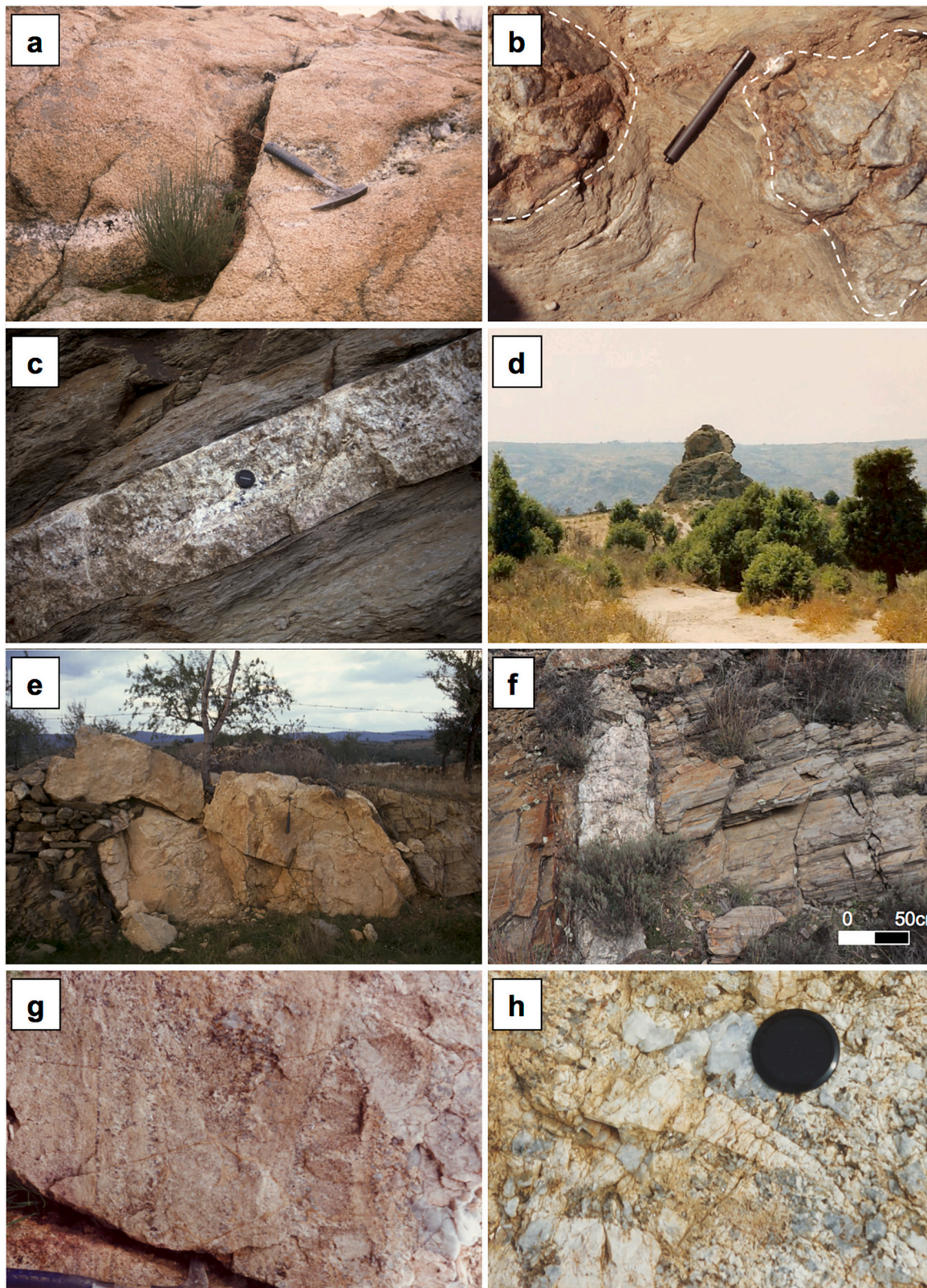
Fig. 3. (a) Intragranitic irregularly elongated barren pegmatite intruded into the MEPL granitic complex (29 T X: 679798 Y: 4539883); (b) quartz-andalusite layer (BP2) concordant to the host-rocks along the S$_3$ foliation, showing strong boudinage (29 T X: 676331 Y: 4538219); (c) simple concordant pegmatitic dyke (29 T X: 681128 Y: 4538904); (d) outcrop of a bulbous aplitic-pegmatitic apophysis (29 T X: 678962 Y: 4538538); (e) K-feldspar-rich subvertical discordant dyke (intermediate pegmatite) showing their characteristic orange hue (29 T X: 678971 Y: 4539939); (f) thin discordant subvertical intermediate dyke (29 T X: 677982 Y: 4539982); (g) vertical layering parallel to the contacts with the hosting metasediments from an intermediate dyke, with alternating aplitic-pegmatitic layers (29 T X: 678517 Y: 4539906); (h) tapered K-feldspar crystal pointing to the contact with the host-rock from an intermediate dyke (29 T X: 678517 Y: 4539906).

(Fig. 3e) comes from the high contents of K-feldspar, with quartz, muscovite and pyrite as minor constituents. (2) *Intermediate pegmatites* represent the most abundant type in the FA field. They outcrop further away to the north of the MEPL granitic complex (between ≈1 and 4 km), generally between the barren and the evolved pegmatites (Fig. 2). Dykes of this type have variable thickness, from <1 m up to a few meters and lengths up to a few hundred meters, with a striking around N010°-030°E and dipping sub-vertically (Fig. 3f). The metasedimentary country rocks show a more or less intense tourmalinization near the contact zone. Layering parallel to the contacts and comb-shaped crystals are frequently observed inside these dykes (Fig. 3g, h). Quartz, albite, K-feldspar and muscovite constitute the main mineral association. Tourmaline, cassiterite, Nb—Ta oxides and phosphates are minor phases.
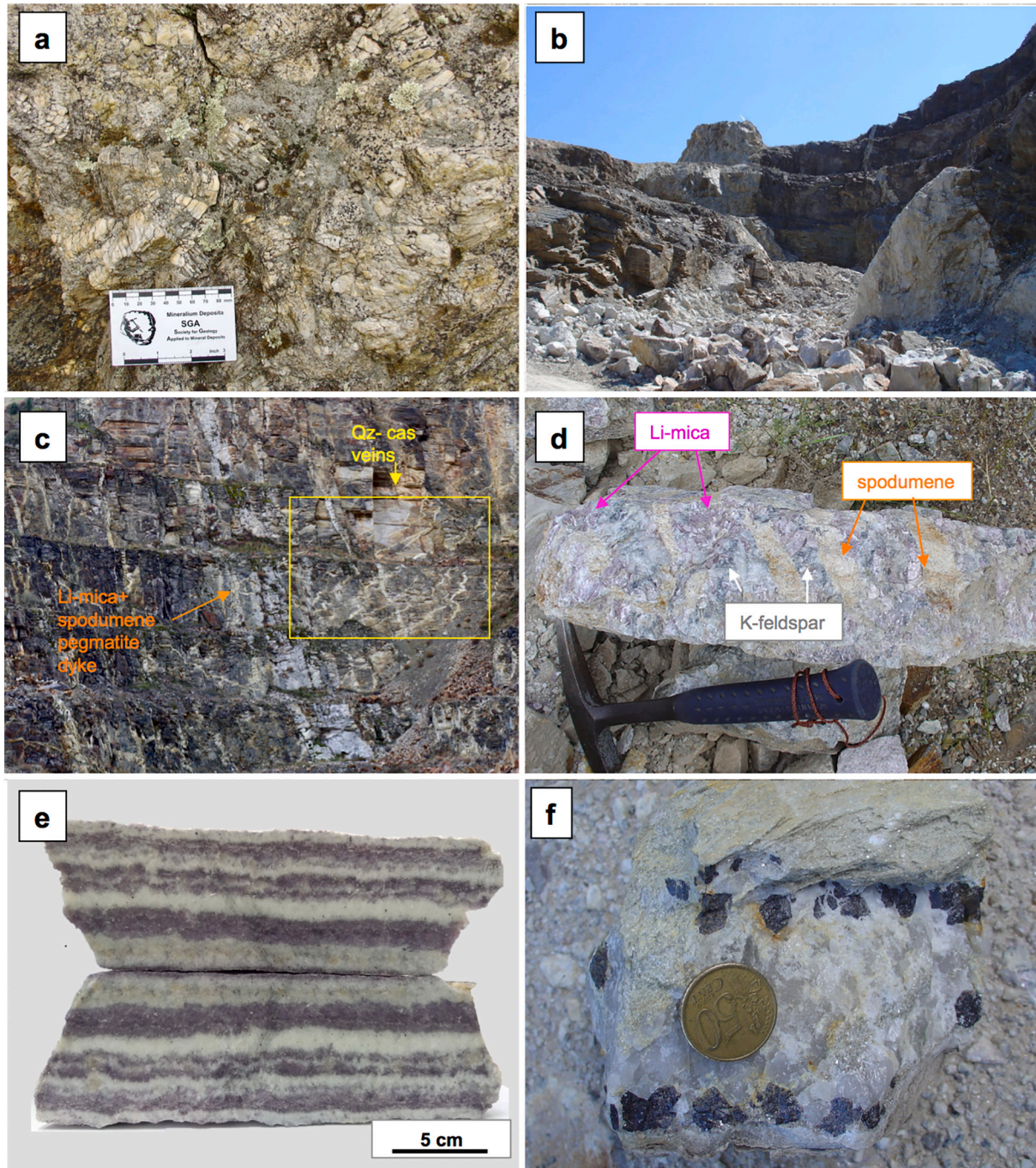

Fig. 4. (a) Petalite-rich subvertical discordant dyke, showing an area with a strong enrichment in petalite (29 T X: 683471 Y: 4541496); (b) spodumene-rich subvertical discordant dyke mined in the Alberto open-pit (29 T X: 681126 Y: 4541933); (c) Main front of the Feli open-pit, where a subvertical discordant Li-mica + spodumene-rich dyke cross-cuts some folded Qz-cas veins (see Fig. 5a, b for more detail) (29 T X: 677681 Y: 4544069); (d) Li-mica, spodumene and greyish K-feldspar decimetric crystals in a hand-sample from a Li-mica + spodumene-rich dyke (same location as c); (e) sample of a Li-mica-rich subvertical discordant dyke (EP4) showing a rhythmic compositional layering, with alternating quartz + Li-muscovite-rich layers and albite-rich ones (29 T X: 675895 Y: 4542153); (f) quartz-cassiterite hydrothermal vein (Qz-cas) showing an internal zonation, with quartz in the core, crystals of cassiterite in an intermediate position and fine-grained muscovite in the contact zone (same location as c).

3.3. Evolved pegmatites

These pegmatites consist of subvertical discordant dykes, enriched in Li ± F (Table 1) and are the most evolved pegmatites in the FA field. According to the Černý and Ercit (2005) classification, they fit in the LCT family, REL-Li sub-class of the Complex type. Tourmalinization is ubiquitous in the contact zones (Errandonea-Martin et al., 2022; Roda et al., 1995a). Four types of evolved pegmatites can be distinguished: (1) *Petalite-rich pegmatites* that are more abundant on the west side of the field (Fig. 2), with thicknesses from 1 m up to ≈ 30 m, lengths up to 1.5 km, and strike around NS to N030°E. Although it is conceivable to recognize zones clearly enriched in petalite inside these dykes (Fig. 4a), it is not possible to identify any internal zonation. The mineral assemblage is very simple and monotonous, with petalite, quartz, albite and K-feldspar as the main minerals, and muscovite as minor phase. A typical example of petalite-rich pegmatites is being mined in the Bajoca open pit (Portugal) (Cardoso-Fernandes et al., 2021) (Fig. 2a). (2) *Spodumene-rich pegmatites* that exhibit a strike, dimension and mineralogy very similar to the previous pegmatite type (Table 1). They are particularly abundant on the east side of the field in the Spanish part (Fig. 2). Spodumene is the dominant aluminosilicate, but petalite appears commonly as a subordinate phase. Besides spodumene and petalite, albite, K-feldspar and quartz constitute the main association, with muscovite as minor phase. Some well-exposed occurrences belonging to this type have been mined in the Alberto open pit (Spain) (Figs. 2a, 4b). (3) There are only three occurrences of *Li-mica + spodumene-rich pegmatites*, in the eastern part of the pegmatite field, at greater distance from the MEPL granitic complex than the previous types (Fig. 2). The best example may be seen in the Feli open pit (Spain) (Figs. 2a, 4c) (e.g., Roda et al., 1996, Roda-Robles et al., 1999). These dykes have lengths up to 500 m and thicknesses ≈ 30 cm to ≈ 20 m, which cross-cut the regional foliation. The mineral assemblage includes quartz, albite, K-feldspar, Li-muscovite and spodumene as main constituents, with muscovite, cassiterite and montebrasite as minor phases (Table 1). These pegmatites do not show an internal concentric zoning. However, a rhythmic compositional layering parallel to the contacts is commonly observed, where quartz- and Li-muscovite-rich layers alternate with albite-rich ones. Spodumene occurs associated with the Li-muscovite and with greyish K-feldspar crystals (Fig. 4d). (4) *Li-mica-rich pegmatites* that are more abundant than the previous ones, also outcropping in the furthest areas from the MEPL granitic complex
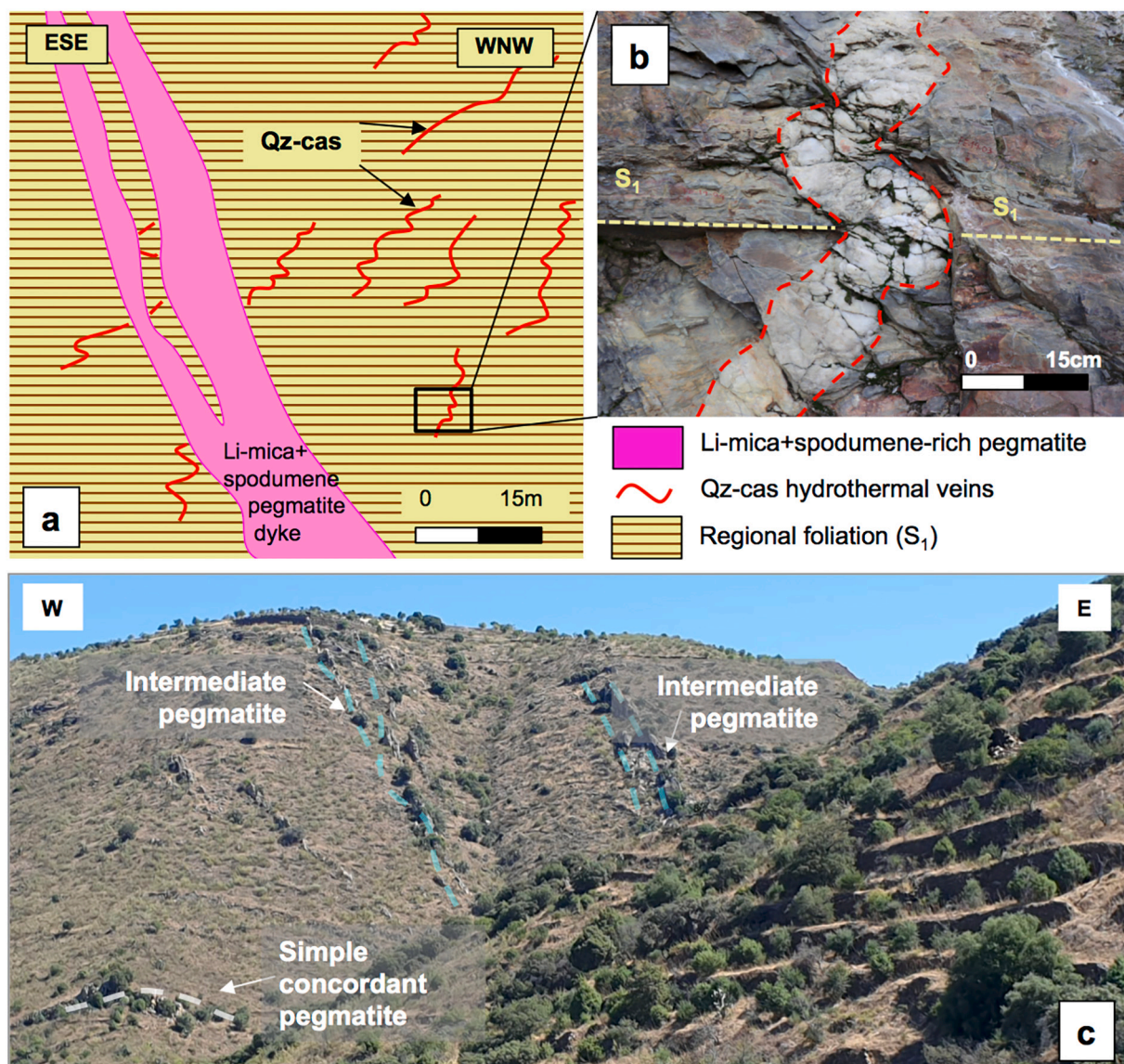

Fig. 5. (a) Sketch of the structural relationships between a Li-mica+spodumene-rich dyke and the vertically folded quartz-cassiterite veins (Qz-cas) in the Feli open-pit; (b) detail of "a" where the relation between the quartz-cassiterite veins and the regional foliation may be observed; and (c) panoramic view of the outcrop of various discordant (N20°E) intermediate subvertical dykes, and a simple concordant pegmatite (N120°E).

(Fig. 2). These dykes, with thickness < 3 m and strike N010°E to N040°E, have quartz, albite, K-feldspar and Li-muscovite as main components. Muscovite, cassiterite, montebrasite and Nb—Ta oxides represent minor phases (Table 1). Some of these pegmatites show a layering parallel to the contacts, quite similar to that observed in the previous pegmatite type (Fig. 4e).

It is noteworthy that the intermediate and the evolved pegmatites share structural, textural and mineralogical features: e.g. (i) all of them are dyke-like sub-vertical bodies, with reduced thicknesses in the same range; (ii) they are subparallel and intrude into the post-D$_3$ latest fractures (NNE-SSW), discordant to S$_1$ schistosity; (iii) they do not show signs of evident deformation and are not affected by the Huebra Shear Zone; (iv) neither concentric internal zoning nor quartz cores are observed in these dykes; (v) often they show UST textures, mainly comb-shaped crystals, together with a subvertical layering parallel to the contacts; (vi) grain size is aplitic in an important proportion of the dykes and giant crystals are very scarce, commonly <12 cm large; and, (vii) metasomatic effects in the country rocks, including tourmalinization and Li, F, Cs, Sn enrichment, are observed in the vicinity of all these dykes.

3.4. Cassiterite-rich quartz veins (Qz-cas)

They are restricted to the north-central portion of the field and were mined for Sn up to the 1970s in the Feli open pit (Figs. 2a, 4c, 5a, b). The veins are discordant to S$_1$. They are folded showing subhorizontal axial planes (Figs. 4c, 5a, b), and show a N020°-040° strike, and a dip in the range 45° to 75° mostly to the SE. They are cross-cut by some unfolded subvertical *Li-mica + spodumene-rich pegmatite* dykes (Figs. 4c, 5a, b). *Qz-cas* veins show thicknesses close to 10 cm (exceptionally up to 50 cm), and show an internal zonation with quartz in the core, crystals of cassiterite in an intermediate position and fine-grained muscovite in the contact zone (Fig. 4f). Quartz, cassiterite and muscovite are the dominant minerals, with albite, microcline and columbite-tantalite group minerals as minor phases (Table 1).

3.5. Spatial distribution of the pegmatite types in the field and structural control

The different pegmatite types from the FA field are not distributed homogeneously in the whole area. The barren pegmatites are intragranitic or outcrop in the vicinity of the MEPL (< 1 km from the contact) (Fig. 2). The number of barren bodies decreases with increasing distance to the MEPL. The most evolved pegmatite types, enriched in Li, F and Sn, outcrop in the furthest zones, concentrated between the MEPL and the Saucelle granites (Fig. 2). The intermediate pegmatites are located between the barren and the most evolved pegmatites. The distance between the barren and the most fractionated pegmatites in the east side of the field (Spain) is up to ≈ 5 km, whereas to the west, in the Portuguese side, the distribution of the different pegmatitic types shows a telescoping, with a much shorter distance between the barren and the Li-rich pegmatitic dykes, usually <2 km (Fig. 2).

The concordant barren dykes (*quartz + andalusite layers* and *simple concordant pegmatites*) are cut by the N020°E fractures where the discordant subvertical dykes (intermediate and Li-rich) are emplaced. These fractures are considered late- to post-D$_3$. They cut also the JPSZ, considered as D$_4$ by some authors (Díez Fernández and Pereira, 2017), whereas the *quartz + andalusite layers*, the *concordant simple pegmatites*, and the main facies of the MEPL granitic complex are affected by the deformation associated with the HSZ (D$_3$), whose last activity ceased at ≈ 307 Ma (Díez Fernández and Pereira, 2017). This shearing apparently did not affect the discordant intermediate and Li-rich dykes, nor the barren *aplitic-pegmatitic apophyses*, the east-MEPL and the Saucelle granites (Dias da Silva, 2014; Gonzalo Corral, 1981). On the other hand, the *Qz-cas* veins occurring in the Feli open-pit are folded and cross-cut by some sub-vertical *Li-mica + spodumene-rich* dykes. The Feli granite also

seems to be cross-cut by the subvertical *Li-mica + spodumene-rich* dykes according to some drilling works.

4. Results

Sampling strategy and analytical methods are explained in the supplementary material.

4.1. Geochronology of pegmatites and granites

A list of the samples dated in this study by Ar/Ar in micas and U/Pb in columbite, with their location, is provided in Supplementary Table 1. ^{40}Ar/^{39}Ar data of mica analyses are given in Supplementary Table 2 and a summarised compilation of obtained ages is shown in Table 2 and Fig. 6. Gas fractions show small variation in the K/Ca ratio, supporting a chemical homogeneity in the samples, displaying only in few samples a relatively high apparent age within the first steps (Fig. 6). Obtained plateau ages comprise about 90% of released gas, with MSWD values of <1.25 (Fig. 6; Supplementary Fig. 1). Overall, pegmatites, the hydrothermal vein and the Feli granite yield an age spectra from 305 to 295 Ma, with coherent inverse isochron ages of 306–295 Ma (Fig. 6 and Supplementary Fig. 1).

In the case of granites, the not-outcropping Feli granite shows an age of 305.0 ± 3.1 Ma; whereas the barren *aplitic-pegmatitic apophyses*, related to the East-MEPL undeformed granitic facies, give an age of 300.4 ± 3.2 Ma (Table 2, Supplementary Table 2, Fig. 6).

For pegmatites, the barren ones located inside (*intragranitic*) or close to the MEPL granite (concordant *quartz + andalusite layers* and *concordant simple pegmatites*), yield ages in the range 302.4 ± 3.4 to 305.2 ± 4.2 Ma, with a mean value of 303.8 ± 3.9 Ma (Table 2, Supplementary Table 2, Fig. 6). Discordant subvertical intermediate and Li-rich pegmatites yield ages in the range 295.1 ± 3.9 to 304.3 ± 4.0 Ma, with a mean value of 299 ± 3.9 Ma (Table 2, Supplementary Table 2, Fig. 6). Finally, *Qz-cas* veins from the Feli open pit are dated with an age of 300.1 ± 3.1 Ma (Table 2, Supplementary Table 2, Fig. 6).

In addition to the Ar/Ar dating of mica, a columbite crystal from a *Li-mica-rich pegmatite* was analysed for dating purposes by U-Th-Pb systematics. This columbite crystal is the largest one found in the FA pegmatites (1 cm long). It is subhedral, free of visible inclusions and metamictic features under optical and electron microscopy observation, and exhibits oscillatory zoning with straight limits among the different sectors (Supplementary Fig. 2). According to its textural features and grain boundary relationships to the associated minerals, this columbite crystal is regarded as an early phase in the crystallization sequence of the pegmatite. U—Pb analyses (Fig. 7, Supplementary Table 3) of this crystal show quite homogeneous concentration of U (mean value 2150 ppm) and Th (mean value 20 ppm) while the concentration of Pb is highly variable over the analysed spots (from 14 to 3300 ppm). The U—Pb ages obtained are mostly concordant although Pb rich spots show discordant values reflecting the presence of previous Pb in those points. 55 out of 62 analysed spots define a linear regression on concordia diagrams that yields a lower intercept at 298 ± 3 Ma ($n = 55$; MSWD = 0.99). However, this regression results in an upper intercept value of ^{207}Pb/^{206}Pb = 0.335 ± 0.012, which points to the possible presence of unresolved microinclusions or Pb loss domains in some analysed spots. In view of this, we have taken into account only the highly concordant results (better than 95%) for the age calculation. This results in an age of 302 ± 3 Ma (^{206}Pb/^{238}U age, $n = 35$; MSWD = 1.1) (Fig. 7), which is regarded as the preferred value for the crystallization of the columbite crystal.

4.2. Geochemistry of pegmatites and granites

Overall, including own data and those compiled from the literature, 23 analyses of intermediate and Li-rich pegmatites have been used in this study. In the case of the granites, the main facies (*syn*—D$_3$), the
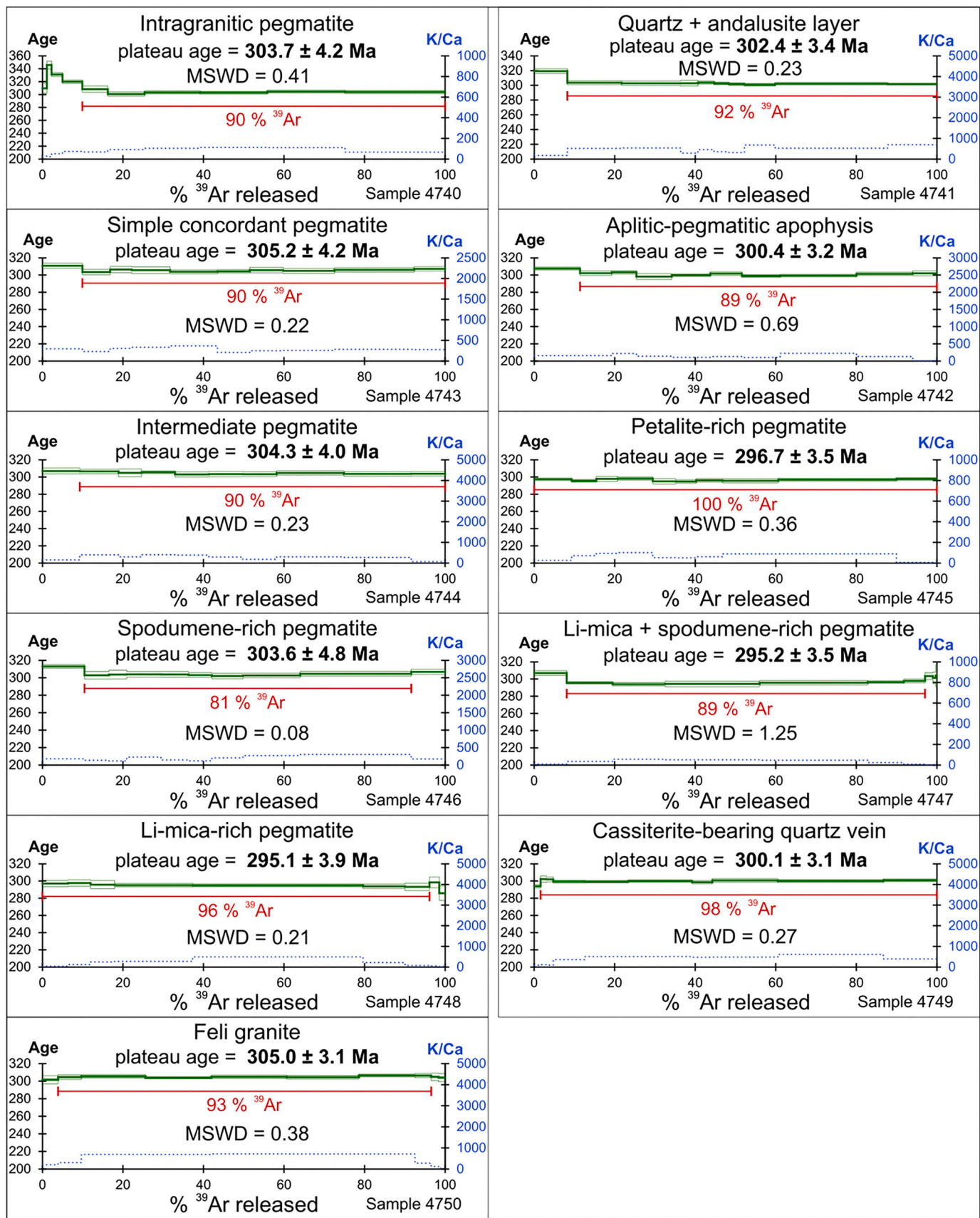
Fig. 6. Plateau ages spectra and summary of isotopic $^{40}Ar*/^{39}Ar$ data of different types of granites and pegmatites of the FA area. The horizontal red line of the image represents the sections of the plateau used in the calculation of the apparent age. MSWD = squared-weighted standard deviation. (For interpretation of the references to colour in this figure legend, the reader is referred to the web version of this article.)
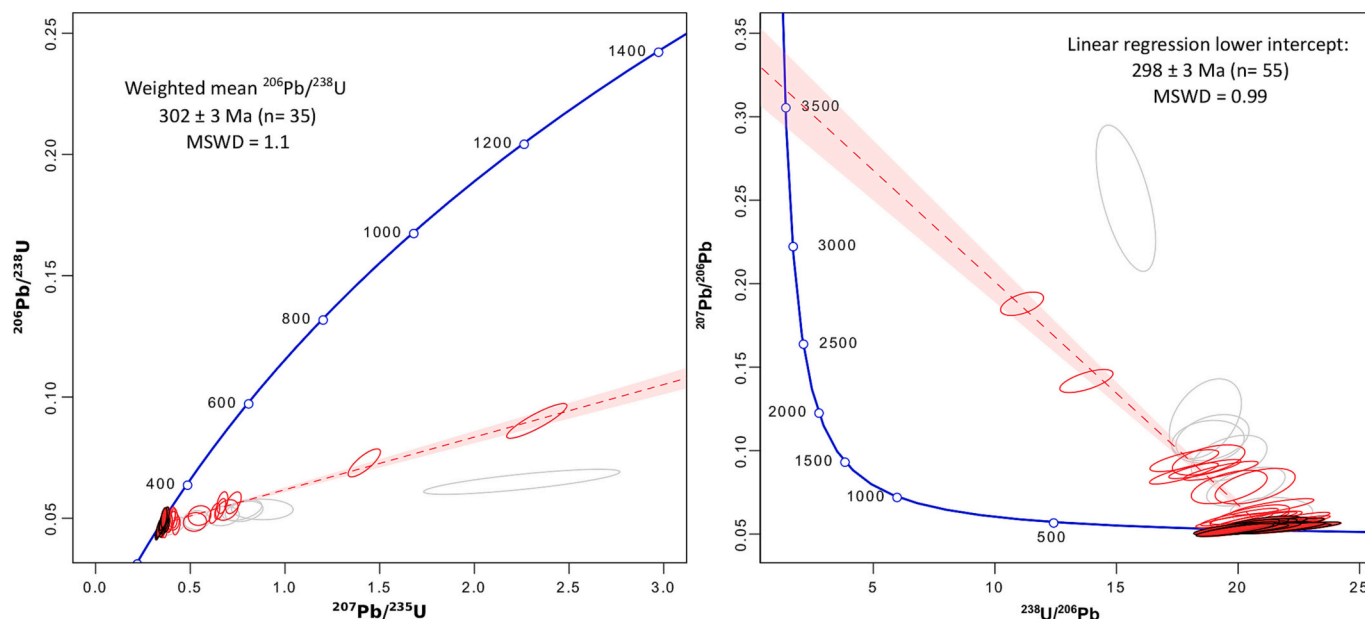
Fig. 7. Concordia diagrams for a columbite crystal from a Li-mica-rich pegmatite dyke. Black border full red ellipses: concordant data (>95%); linear regression in dotted red line calculated with red ellipses; grey ellipses: not used data. (a) Wetherill Concordia diagram and weighted mean $^{206}Pb/^{238}U$ for concordant analysis; and, (b) Tera-Wasserburg Concordia diagram and age defined by lower intercept of linear regression stablished by red ellipses. (For interpretation of the references to colour in this figure legend, the reader is referred to the web version of this article.)

Table 2
Summary of the ages obtained by Ar/Ar in micas for the different pegmatite types, the cassiterite-rich quartz veins from the FA area and of the not-outcropping Feli granite.

Lithotype	Plateau age
	(± 1 σ) (Ma)
Intragranitic pegmatite	303.7 ± 4.2
Quartz + andalusite layer	302.4 ± 3.4
Simple concordant pegmatite	305.2 ± 4.2
Aplitic and pegmatitic apophyses	300.4 ± 3.2
Intermediate pegmatite	304.3 ± 4.0
Petalite-rich pegmatite	296.7 ± 3.5
Spodumene-rich pegmatite	303.6 ± 4.8
Li-Mica + spodumene-rich pegmatite	295.2 ± 3.5
Li-mica-rich pegmatite	295.1 ± 3.9
Cassiterite-rich quartz hydrothermal vein	300.1 ± 3.1
Feli granite (not outcropping)	305.0 ± 3.1

undeformed facies (East-MEPL), and a mixed facies of the MEPL granitic complex; the main facies and the marginal facies of the Saucelle granite, and one drilling sample of the Feli granite have been analysed (Table 3).

The analysed pegmatites are highly peraluminous, with significant differences among different dykes and, in most cases, with a higher peraluminosity than the granites of this area (Table 3, Fig. 8a, b). No relationship has been found among major element contents and the pegmatite type, whereas significant chemical differences exist among the different granitic facies and between pegmatites and granites (Fig. 8). All the analysed pegmatites show higher Al contents than the granites from this area, with broad variations among them (Fig. 8a, b, c). Nevertheless, the most important variations among major elements for the pegmatites are those of SiO₂, in many cases with values lower than those of the granites (Fig. 8c, d, e, f, g). Opposite to granites, most of the pegmatites are richer in Na than in K, with just a few exceptions (Fig. 8h). Iron and Mg contents are relatively low for the granites, and even lower in the pegmatites (Fig. 8d, e). Calcium contents in all granites of this area are relatively low (<0.67 wt% CaO) (Fig. 8f), typical of the two-mica leucogranitic series or the P-rich, Ca-poor monzogranitic series from the CIZ. With a few exceptions, Ca contents in the pegmatites

are even lower (Fig. 8f). Titanium contents are also relatively low for the granites and even lower for the pegmatites (Fig. 8g). All granite samples have relatively high P contents (0.25–0.91 wt% P₂O₅) (Fig. 8b). Therefore, they may be classified as perphosphorus granites. The P₂O₅ contents in pegmatites exhibit a broader range, with some values significantly higher than those of the granites (Fig. 8b). The three units of the MEPL granitic complex show chemical differences regarding the major and minor elements, with the late undeformed unit (East-MEPL) being the richest one in Si, Al and P, and the poorest in Fe, Mg, Ti and Ca (Fig. 8). In the case of the Saucelle granite, the marginal facies is also richer in Si, Al and P and poorer in Fe, Mg and Ti than the main Saucelle facies (Fig. 8). Therefore, according to their major elements chemistry, the main facies of the MEPL may be included in the two-mica leucogranitic series; whereas the other granitic units in the area (East-MEPL, Saucelle and Feli) may be included in the series of perphosphorus, highly peraluminous and Ca-poor monzogranites, both series with a metasedimentary source (e.g. Roda-Robles et al., 2018; Villaseca, 2011).

Regarding the trace elements, when compared with the UCC mean values (Rudnick and Gao, 2014), overall the FA granites and pegmatites are enriched in Li, Cs, Rb, Sn, Be, Tl, Ta and P; and depleted in Ba, Th, REE Hf, Zr, Ti and Y (Table 3; Fig. 9a). Granites are richer in U than the UCC, whereas pegmatites are poorer. The opposite behaviour is observed for Nb, which is enriched in pegmatites in relation to the UCC, while granites are depleted. Fluorine and B in some cases appear depleted in the studied pegmatites. Nevertheless, it is needed to take into account the important metasomatism observed in the hosting micaschists of most of the intermediate and Li-rich pegmatites, which includes tourmalinization and a notorious increase in the Li, F, Cs and Sn contents in the halo around these pegmatitic bodies (Errandonea-Martin et al., 2022). This most probably means that the original contents of the pegmatitic melts in F, B, Li, Cs and Sn, were higher than those presented by the pegmatites nowadays.

Besides the important differences observed in the trace elements contents between granites and pegmatites, there are significant variations for some of them in relation to the pegmatite type. Pegmatites are, in general, richer in Li, Rb, F, Sn, Be, Tl, Nb, Ta, Ge, and Ga; and poorer in Ba, Th, U, REE, Zr and Y than the granites (Table 3, Fig. 9). Pegmatites also tend to be richer in B and Cs than the MEPL and Saucelle granites,

Table 3

Whole-rock major (wt%) and trace-element (ppm) composition of the different granitic units of the Fregeneda-Almendra area and of the intermediate, petalite-rich, spodumene-rich and Li-mica + spodumene-rich pegmatites, and of the different granites from the FA. MEPL = Mêda-Escalhão-Penedono-Lumbrales granitic complex. *Data taken from Errandonea-Martin et al. (2022). **Data taken from Roda-Robles et al. (2018).

	GQ-XX-06	GQ-XX-05	GQ-XX-07	GQ-XX-13	GQ-XX-12	GR-FELI	BAR-19	BAR-06*	PET-01*	ALB-02	ALB-01*	FRG-RT-ALB**	FEL-02*	FRG-RT-Li**
X coordinates (29 T)	685,853	685,994	685,848	685,199	684,586	677,681	678,383	678,016	683,499	681,138	681,110	681,126	677,619	675,895
Y coordinates (29 T)	4,534,243	4,535,038	4,534,259	4,545,381	4,544,848	4,544,069	4,541,975	4,539,988	4,541,514	4,541,950	4,542,021	4,541,933	4,543,772	4,542,153
lithology	granites						pegmatites							
lithotype	MEPL	MEPL	East-MEPL	Saucelle	Saucelle	Feli	Intermediate		Petalite-rich	Spodumene-rich			Li-mica+spodumene-rich	
	main	mixed	late	main	marginal	metasomatized								
SiO2	72.83	72.65	73.21	73.13	74.23	73.44	69.8	71.04	74.29	67.61	74.27	73.31	70.84	70.14
Al2O3	14.79	14.69	14.86	14.6	15.01	15.09	17.74	15.91	15.3	19.82	16.79	16.72	17.07	16.22
Fe2O3t	1.92	1.82	1.45	1.52	0.92	1.44	0.33	0.5	0.38	0.49	0.36	0.54	0.45	0.25
MnO	0.021	0.018	0.024	0.02	0.014	0.031	0.077	0.041	0.027	0.027	0.017	0.035	0.03	0.068
MgO	0.4	0.42	0.29	0.31	0.18	0.26	0.04	0.05	0.01	0.05	0.15	0.13	0.04	0.73
CaO	0.67	0.65	0.53	0.6	0.62	0.66	0.29	0.3	0.43	0.17	0.21	0.99	0.32	1.71
Na2O	3.03	3.35	2.92	3.17	3.18	3.29	4.78	3.44	5.41	3.37	2.44	4.66	6.3	5.51
K2O	5.21	5.62	5.56	5	4.69	4.84	5.08	7.46	3.78	7.25	3.74	1	2.15	2.12
TiO2	0.262	0.239	0.149	0.177	0.117	0.16	0.01	0.02	0.02	0.02	0.02	0.015	0.02	0.008
P2O5	0.42	0.35	0.5	0.41	0.42	0.52	0.82	0.67	0.48	0.35	0.37	0.79	0.82	0.68
LOI	0.89	0.66	1.11	0.98	1.03	0.97	1.06	0.63	0.71	0.65	0.86	0.96	1.00	2.90
Total	100.44	100.47	100.60	99.92	100.41	100.70	100.03	100.06	100.84	99.81	99.23	99.15	99.04	100.34
F	400	400	700	400	400	2300	700	200	100	100	<100	500	3100	3700
B	26	25	20	17	14	165	40	< 10	50	30	20	13	50	54
Li	110	100	150	110	70	870	686	61	200	3700	9070	7570	2600	2660
Be	5	4	9	10	12	7	108	71	89	18	94	135	208	203
Sc	3	2	2	2	2	2	0.1	0.2	0.1	< 0.1	0.1	< 1	< 0.1	< 1
V	10	12	< 5	6	< 5	6	< 5	< 5	< 5	< 5	< 5	< 5	< 5	< 5
Cr	< 20	< 20	< 20	< 20	< 20	< 20	70	70	100	70	70	130	70	40
Co	2	3	1	1	1	1	0.7	0.9	0.6	1.2	0.6	< 1	1.3	< 1
Ni	< 20	40	< 20	< 20	< 20	< 20	30	20	40	30	30	< 20	30	< 20
Cu	< 10	< 10	< 10	< 10	< 10	< 10	6	12	8	31	10	< 10	27	< 10
Zn	110	70	60	50	30	70	80	40	40	40	50	60	< 30	110
Ga	23	21	21	21	24	20	41.5	19.6	15.7	19.2	15.1	20	38.2	38
Ge	1.3	1.3	1.3	1.5	1.4	2	8	4.1	4.1	4.6	4	4.7	13.6	9.9
As	< 5	< 5	< 5	< 5	< 5	27	< 5	< 5	7	< 5	< 5	< 5	7	< 5
Rb	284	306	336	361	358	465	2150	1310	640	1310	772	214	1080	1070
Sr	62	74	47	58	36	67	80	45	82	55	50	135	75	154
Y	8.8	7.1	5.5	6.1	6.5	6.9	1.7	1.4	0.6	0.7	0.6	0.8	0.2	0.2
Zr	101	89	54	65	50	68	28	7	11	2	3	8	38	20
Nb	9.1	7.6	9.3	8.2	8.3	10.9	141	10.3	12.6	9.8	22.1	18.5	78.1	56.3
Mo	< 2	< 2	< 2	< 2	< 2	< 2	< 1	2	2	< 1	1	< 2	< 1	2
Ag	< 0.5	< 0.5	< 0.5	< 0.5	< 0.5	< 0.5	–		–	–		< 0.5	–	0.5
In	0.1	0.1	0.1	0.1	0.1	0.1	< 0.2	< 0.2	< 0.2	< 0.2	< 0.2	0.3	< 0.2	1.2
Sn	7	8	13	17	15	76	284	34.6	61.1	52.6	93.2	71	768	350
Sb	< 0.2	< 0.2	< 0.2	< 0.2	< 0.2	< 0.2	< 2	< 2	< 2	< 2	< 2	< 0.2	< 2	< 0.2
Cs	14.9	14.2	24.2	33.8	18.5	190	51.6	40.7	28.5	52.7	57.2	26.6	379	236
Ba	215	283	164	196	85	187	69	29	52	45	20	18	27	67
La	29.5	22.4	10	15.5	12.4	15.4	0.9	0.7	< 0.4	< 0.4	0.6	0.67	< 0.4	0.44
Ce	69.3	50	21.7	33.6	27.8	34.2	1.1	0.9	< 0.8	< 0.8	< 0.8	1.24	< 0.8	0.78
Pr	8.51	5.94	2.52	3.92	3.19	4.03	0.2	< 0.1	< 0.1	< 0.1	0.1	0.13	< 0.1	0.11
Nd	32.4	23.1	9.62	14.4	12.2	15.3	0.6	0.7	0.6	< 0.4	0.5	0.5	< 0.4	0.39
Sm	6.85	5.27	2.58	3.72	3.36	3.68	0.2	0.2	< 0.1	< 0.1	0.2	0.11	< 0.1	0.03
Eu	0.485	0.538	0.292	0.393	0.244	0.321	< 0.1	< 0.1	< 0.1	< 0.1	< 0.1	0.033	< 0.1	0.038

13

Table 3 (*continued*)

	GQ-XX-06	GQ-XX-05	GQ-XX-07	GQ-XX-13	GQ-XX-12	GR-FELI	BAR-19	BAR-06*	PET-01*	ALB-02	ALB-01*	FRG-RT-ALB**	FEL-02*	FRG-RT-Li**
X coordinates (29 T)	685,853	685,994	685,848	685,199	684,586	677,681	678,383	678,016	683,499	681,138	681,110	681,126	677,619	675,895
Y coordinates (29 T)	4,534,243	4,535,038	4,534,259	4,545,381	4,544,848	4,544,069	4,541,975	4,539,988	4,541,514	4,541,950	4,542,021	4,541,933	4,543,772	4,542,153
lithology	granites						pegmatites							
lithotype	MEPL	MEPL	East-MEPL	Saucelle	Saucelle	Feli	Intermediate		Petalite-rich	Spodumene-rich			Li-mica+spodumene-rich	
	main	mixed	late	main	marginal	metasomatized								
Gd	3.96	3.35	2.12	2.89	2.53	2.49	0.3	0.2	< 0.1	< 0.1	< 0.1	0.13	< 0.1	0.08
Tb	0.51	0.43	0.32	0.39	0.39	0.35	< 0.1	< 0.1	< 0.1	< 0.1	< 0.1	0.02	< 0.1	< 0.01
Dy	2.18	1.85	1.41	1.66	1.74	1.66	< 0.3	< 0.3	< 0.3	< 0.3	< 0.3	0.14	< 0.3	0.05
Ho	0.29	0.23	0.17	0.21	0.2	0.22	< 0.2	< 0.2	< 0.2	< 0.2	< 0.2	0.03	< 0.2	< 0.01
Er	0.64	0.49	0.38	0.41	0.43	0.51	< 0.1	< 0.1	< 0.1	< 0.1	< 0.1	0.08	< 0.1	0.04
Tm	0.075	0.059	0.048	0.051	0.05	0.065	< 0.1	< 0.1	< 0.1	< 0.1	< 0.1	0.009	< 0.1	0.005
Yb	0.43	0.34	0.3	0.28	0.26	0.42	< 0.1	0.2	< 0.1	< 0.1	< 0.1	0.06	< 0.1	0.03
Lu	0.067	0.048	0.042	0.034	0.039	0.058	< 0.01	0.01	< 0.01	< 0.01	0.08	0.009	0.02	0.005
Hf	2.7	2.5	1.5	1.8	1.5	1.9	2.3	0.4	0.6	<0.2	<0.2	0.3	4.8	1.8
Ta	1.68	4.39	1.99	1.68	1.9	4.12	169	3.5	6.7	7.6	14	10.9	118	81.7
W	1.7	10.4	6	2.5	2.4	5	3.3	3	0.9	1.2	< 0.7	< 0.5	3.9	5.8
Tl	1.62	1.73	1.88	1.96	1.92	2.73	18.3	10.4	4.3	9.8	6.2	1.17	7.7	6.54
Pb	27	31	23	20	20	24	13.7	13.4	35	27.7	12.7	9	20.2	30
Bi	0.5	0.4	0.6	0.9	0.6	0.7	< 2	< 2	< 2	< 2	< 2	0.2	< 2	0.5
Th	23.6	14.3	4.37	7.32	5.71	8.88	0.9	0.2	0.2	0.1	0.4	0.77	3.1	2.03
U	11.8	8.9	6.38	8.08	8.28	11.6	2.5	1.2	1.7	0.9	1.5	2.33	8.9	8.62
K/Rb	152	152	137	115	109	86	20	47	49	46	40	39	17	16.4
A/(CNK)	1.2	1.1	1.3	1.2	1.3	1.3	1.3	1.1	1.1	1.4	2.0	1.6	1.3	1.1
Nb/Ta	5.4	1.7	4.7	4.9	4.4	2.6	0.8	2.9	1.9	1.3	1.6	1.7	0.7	0.7
Zr/Hf	37.4	35.6	36.0	36.1	33.3	35.8	12.2	17.5	18.3	–	–	26.7	7.9	11.1
(La/Lu)N	45.7	48.4	24.7	47.3	33.0	27.6	–	7.3	–	–	0.8	7.7	–	9.1
Eu/Eu*	0.0	0.0	0.0	0.0	0.0	0.0	–	–	–	–	–	0.1	–	0.2
ΣLREE	138.1	100.8	43.9	67.2	55.8	68.6	2.8	2.5	–	–	–	2.5	–	1.6
ΣHREE	7.3	6.1	4.3	5.3	5.0	5.1	–	–	–	–	–	0.4	–	0.2

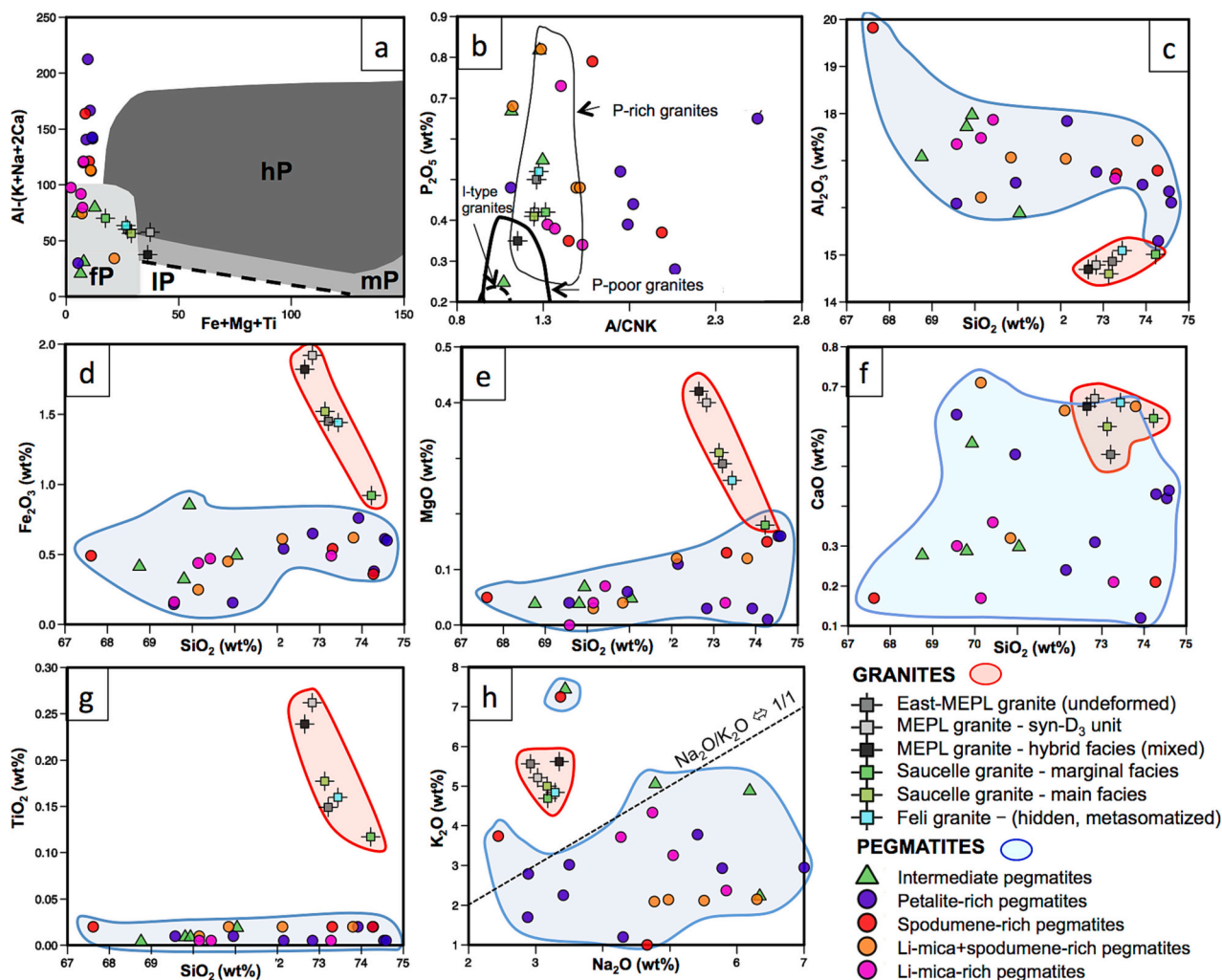* From Errandonea-Martin et al. (2022).

** From Roda-Robles et al. (2018).

Fig. 8. (a) Composition of granites and pegmatites from the FA area in the A–B diagram of Debon and Le Fort (1983), where A = Al-(K + Na + 2Ca) and B = Fe + Mg + Ti, in mmol values, modified by Villaseca et al. (1998b), (hP = high peraluminous; mP = medium peraluminous; lP = low peraluminous; fP = felsic peraluminous); (b) A/CNK (molar Al_2O_3/(CaO + NaO + K_2O)) vs P_2O_5 (in wt%) of the FA granitic and pegmatitic rocks. The three discriminant fields are modified from Villaseca et al. (2008); c. to g. Harker diagrams for the granites and pegmatites from the FA area: (c) SiO_2 vs Al_2O_3; (d) SiO_2 vs $Fe_2O_{3(tot)}$; (e) SiO_2 vs MgO; f. SiO_2 vs CaO; (g) SiO_2 vs TiO_2; and, h. Na_2O vs K_2O.

whereas the metasomatized Feli granite is richer in B than most of the analysed pegmatites, and richer in Cs and F than the *intermediate, petalite-rich* and *spodumene-rich pegmatites*. The highest Li values are presented by the Li-aluminosilicate-rich bodies (*petalite-rich* and *spodumene-rich*) (up to 7090 and 9070 ppm Li respectively) (Table 3, Fig. 9b); whereas F is most elevated in the *Li-mica + spodumene-rich pegmatites* and, especially, in the *Li-mica-rich pegmatites* (Table 3, Fig. 9b). The Li-mica-rich pegmatites are also the richest ones in Cs, Rb, Sn, Be, Ta, Ge and Ga, showing the lowest K/Rb ratios (Table 3, Fig. 9). A good positive correlation is presented by all the analysed rocks for Sn, Nb + Ta, Cs, Be, Ge and Tl, with an overall gradual enrichment from the granites, through the intermediate and the Li-aluminosilicate-rich bodies, up to the Li-mica-rich pegmatites (Fig. 9). This enrichment is parallel to a decrease in the K/Rb ratio.

There are also important differences in the content of some trace elements between the metasomatized Feli granite and the other granites in the area (MEPL and Saucelle) (Table 3, Fig. 9). Main differences are the higher Li, F, Cs and B content of Feli granite, and the lowest K/Rb ratio. As for the major and minor elements, there are also significant variations in the trace element contents for the three units of the MEPL, with the highest Li, Rb, Cs, Be, Sn and F, and the lowest Ba, Sr, Th, U and REE contents in the late facies (East-MEPL). These values are, in general,

closer to those of the Saucelle main and marginal facies than to those of the *syn*-D_3 and hybrid facies of the MEPL (Table 3, Fig. 9).

5. Discussion

5.1. Pegmatites from the FA field: single or multiple fractionation trends?

Six of the 10 pegmatite types from the FA (the two intermediate and the four Li-rich pegmatite types) share structural (e.g. shape, size, strike, dipping and relationships to deformation); textural (e.g. common aplitic facies, UST and layering); and mineralogical features. In addition, they show the same relationship to the country rock, all of them cross-cutting the schistosity and developing strong B-Li-F-metasomatism in the vicinity of all these dykes. In addition to these common features, a gradual chemical transition with an overall continuous increase in Li, F, Rb, Cs, Be, Nb + Ta, Sn, Ge and Tl, parallel to a decrease in the K/Rb ratio (Table 3; Figs. 8, 9), following the sequence: *intermediate → petalite-rich and spodumene-rich → Li-mica + spodumene-rich and Li-mica-rich*, is observed at whole-rock scale. Continuous and gradual chemical variations from intermediate to Li-mica-rich pegmatites are also reflected by minerals such as feldspars (Vieira, 2010); micas (Roda et al., 1995b; Vieira et al., 2011); phosphates (Roda et al., 1996; Roda-Robles et al.,
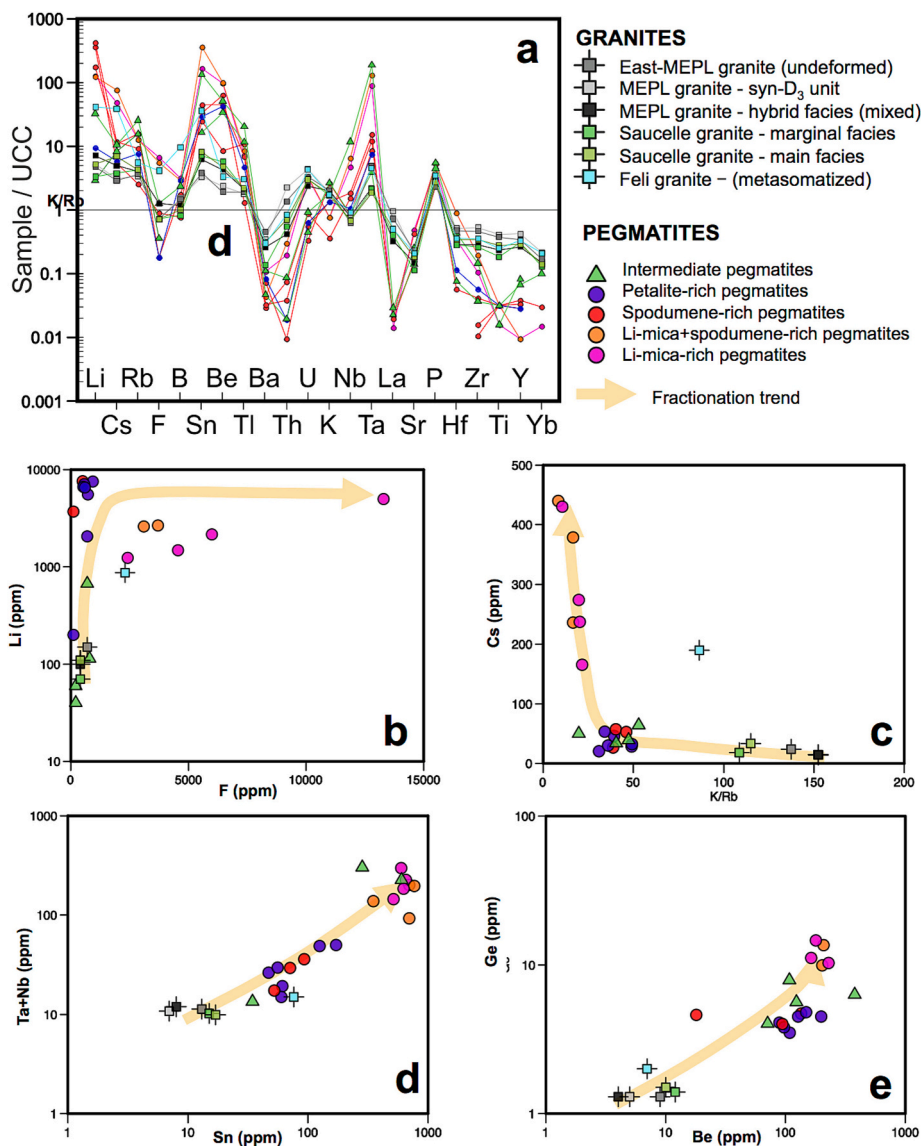
Fig. 9. (a) Spider plots for the FA granites and intermediate and Li-rich pegmatites normalized to Upper Continental Crust (UCC; Rudnick and Gao, 2014); (b) to (e) Selected trace element (ppm) variation diagrams for the FA granites, and intermediate and Li-rich pegmatites. Beige arrow = possible fractionation trend for the granites and intermediate and Li-rich pegmatites.

2010); and tourmaline (Roda et al., 1995a). All these facts strongly suggest that the two types of intermediate pegmatites and the four types of Li-rich pegmatites form part of the same fractionation trend.

The rest of the pegmatites show different structural features and, in general, different relationships to deformation. The similar area of outcrop, equal relationship to deformation and to the host-rock, suggest that the concordant *quartz + andalusite layers* and the *simple concordant pegmatites* may be cogenetic, and clearly independent from the discordant intermediate and Li-rich pegmatites. Regarding the barren *aplitic-pegmatitic apophyses*, their relation to deformation (they cross-cut the HSZ structures) together with the important differences in their structure and texture, indicate that they are not related to the concordant *quartz + andalusite layers* neither to the *simple concordant* pegmatites.

Therefore, in the FA field pegmatites belonging to different fractionation trends coexist, the most important trend (volumetrically and economically) corresponding to that of the subvertical discordant intermediate and Li-rich pegmatite dykes.

5.2. Pegmatitic melts in the FA field: fractional crystallization or partial melting?

Barren pegmatites are not included in this point of the discussion as they belong to a different pegmatitic event, as stated in the previous section.

The derivation of LCT rare-element pegmatites from peraluminous granitic melts via fractional crystallization is the most common model for several worldwide pegmatite fields (e.g., Breiter et al., 2021; Černý, 1992; Garate-Olave et al., 2020; London, 2008). However, an anatectic origin for the pegmatitic melts has also been suggested in a good number of cases (e.g., Norton, 1973; Novák et al., 2013; Simmons et al., 2016; Sokolov, 1982; Webber et al., 2019). In the case of the FA intermediate and Li-rich pegmatites, there are several arguments supporting a fractionation model for them: (1) The continuous chemical changes from granite, through intermediate, up to the Li-richest pegmatites. This trend is observed in other pegmatite fields and granitic cupolas from the CIZ, where a progressive change from granitic to highly evolved pegmatitic facies is shown (e.g. Breiter et al., 2021; Garate-Olave et al., 2020; Roda-Robles et al., 2012). (2) A time gap of about >10 Ma exists between the
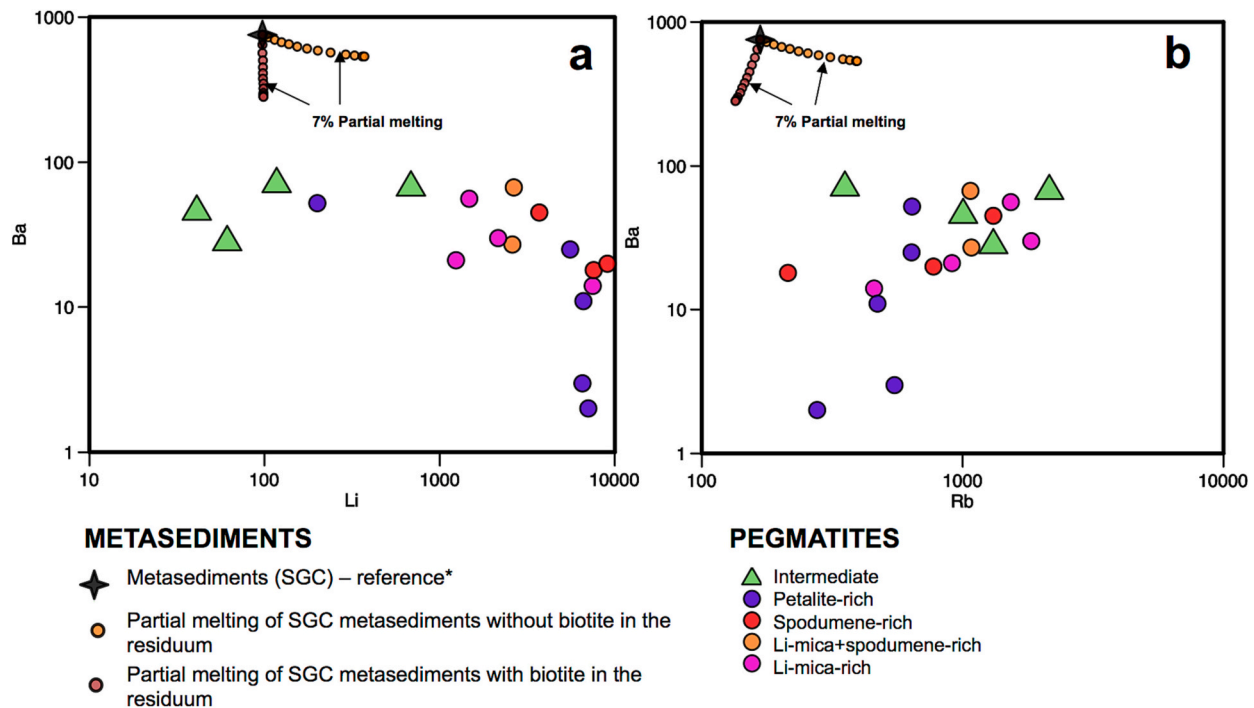
Fig. 10. Plot of a. Li vs Ba, and b. Rb vs Ba, for the intermediate and evolved Li-rich pegmatites from the FA area; together with the possible paths of partial melting of the SGC metasediments with and without biotite in the residuum. The black star corresponds to the mean composition of metasediments not affected by metasomatism from the pegmatites (from Errandonea-Martin et al., 2022).

(D_2) migmatites and extensional fabrics from the region (325–320 Ma, Valverde-Vaquero et al., 2007; Rubio-Pascual et al., 2014; Martins et al., 2020) and the late- to post-D_3 intermediate and Li-rich pegmatites from FA (304–295 Ma) (Figs. 6, 7). (3) The low-grade metamorphic nature of host-rocks of these intermediate and Li-rich pegmatites, with P-T conditions far from anatexis. (4) Although they are not conclusive facts, the spatial relationship of pegmatites with granite bodies (Fig. 2), as well as their ages in the same ranges, support their genetic link. (5) The chemical composition of intermediate and Li-rich pegmatites and that of the minimum melt fractions of anatectic areas show important differences (e.g. Barbero et al., 1995; Milord et al., 2001; Sawyer, 2020) (Table 3). Taking into account that SGC metasediments have often been considered the source of the two mica leucogranites and of the perphosphorous, Ca-poor monzogranitic suites in the CIZ (e.g., Antunes et al., 2008; Bea et al., 1999, 2003; Errandonea-Martin et al., 2019; Ferreira et al., 2019, 2020; Roda-Robles et al., 2018), a partial melting modelling starting from these materials has been made and the results presented in Fig. 10. Distribution coefficients used in this modelling are provided in Supplementary Table 4. According to the obtained results, melting of SGC materials could not produce directly melts with the Li and Rb concentrations observed in the Li-rich pegmatites from the FA field (Fig. 10). Taking into account the melting threshold of 7% needed for the partial melts to start moving (Rosenberg and Handy, 2005), in the best of the cases, i.e., without biotite in the residuum combined with low proportions of partial melting (>7%) of the SGC materials, the amounts of Li and Rb of such melts would be <311 ppm and < 360 ppm respectively. That is, far from the Li and Rb contents shown by the FA Li-rich pegmatites (Fig. 10). Consequently, an anatectic origin for the pegmatitic melts related to the intermediate and Li-rich pegmatites from the FA field may be ruled out. In contrast, a mechanism of fractional crystallization of a granitic melt seems to be the most realistic option for the generation of such pegmatitic melts. Actually, the S-type granites distinguished in the FA area (MEPL, East-MEPL, Saucelle and Feli), belong to the series that have been proposed as parental melts for other Li-rich pegmatites from the CIZ, i.e., to the two-mica peraluminous leucogranitic series (MEPL) or to the peraluminous, perphosphorous,

Ca-poor monzogranitic series (Saucelle, East-MEPL and Feli) (e.g. Roda-Robles et al., 2018).

5.3. Temporal relationships between granites, pegmatites and Variscan deformation in the FA field

Geochronological and geological data indicate that there was an important and nearly continuous magmatic activity in the FA from ≈ 320 to 295 Ma, i.e., during *syn*- to post-D_3 Variscan deformation stages. In the case of LCT flux-rich pegmatite tabular bodies with reduced thicknesses, the cooling and crystallization time will never be greater than the calculated standard-deviation error of the apparent age, as demonstrated by the work of Webber et al. (1999). So, as stated by Hanes (1991), the apparent plateau ages obtained for the FA pegmatite dykes are presumed to represent the crystallization age of these pegmatites.

The oldest igneous lithologies in the FA area correspond to the main facies of the MEPL granite, with U—Pb in zircon ages in the range of 313-319 Ma (Ferreira et al., 2019; Pereira et al., 2018), thus compatible with the syn-D_3 granitoids of the two-mica leucogranitic series (Fig. 11). The ages obtained for the *intragranitic pegmatites* and the barren concordant *quartz + andalusite layers* and *simple concordant pegmatites* are somehow younger, with values in the range of 302.4 ± 3.4 to 305.2 ± 4.2 Ma (Table 2, Fig. 6). However, as explained above, field relationships with the syn-D_3 MEPL facies, as well as their structural features, indicate that the obtained Ar/Ar age for the concordant dykes (*quartz + andalusite layers* and *simple concordant pegmatites*) is clearly too young. We speculate that the effects of the HSZ over these dykes, which caused mylonitization and boudinage on them, could have opened the Ar/Ar system of the dated micas, which closes at relatively low temperatures (≈390–440 °C, Harrison et al., 2009) resetting the Ar/Ar system and leading, thus, to younger ages for them, corresponding to the latest activity of the HSZ.

The next magmatic event would be the intrusion of the Feli granite to the north of the FA area (Fig. 11), which presents a plateau age of 305.0 ± 3.1 Ma. This age, together with its geochemical features, suggest that
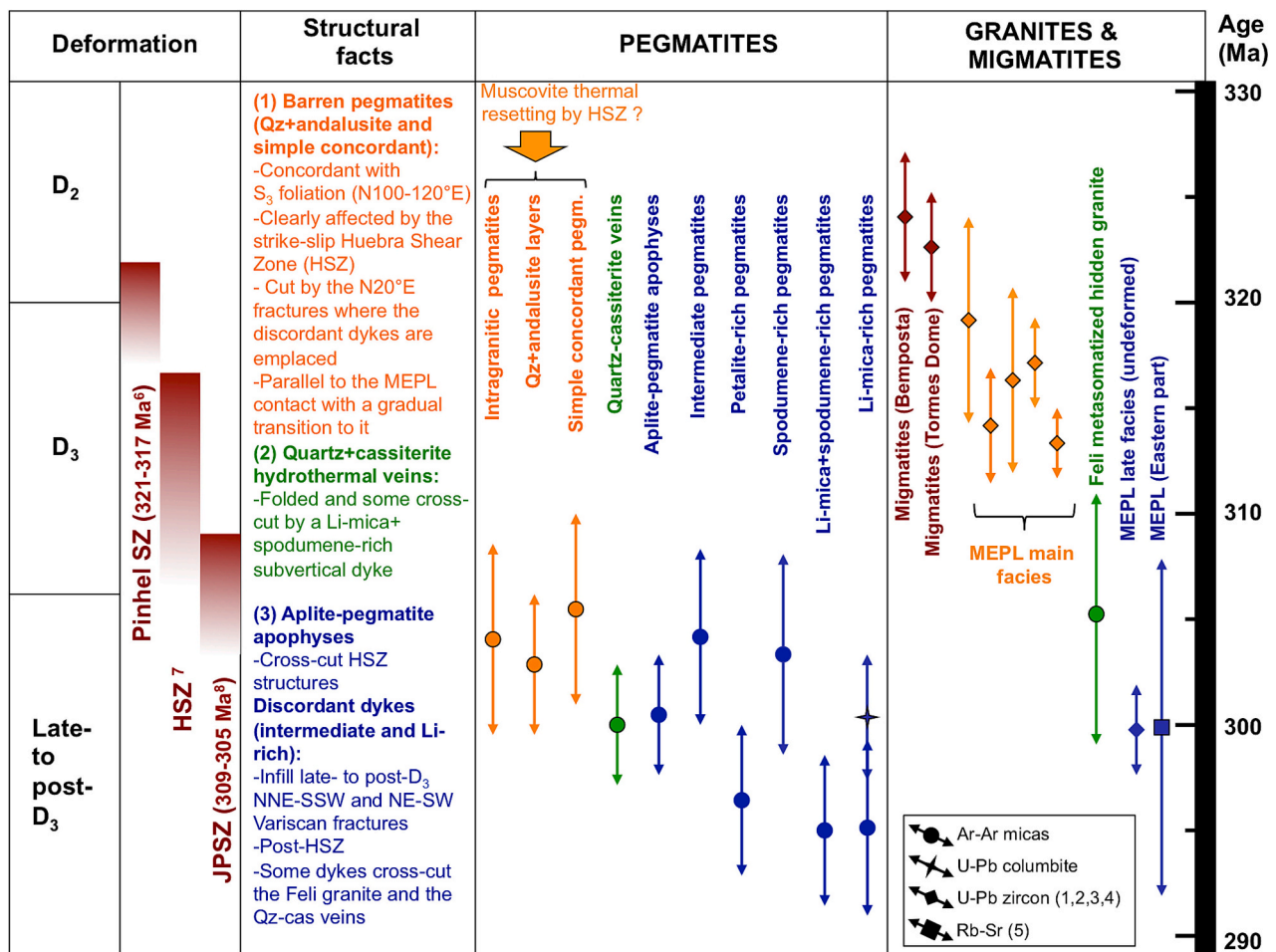
Fig. 11. Compilation of the available geochronological data on the granites and pegmatites of the FA area as well as main geological facts. The three different colors (orange, green and blue) correspond to different magmatic-mineralizing events according to the model proposed in this study. References: (1) Pereira et al. (2018); (2) Ferreira et al. (2019); (3) Martins et al. (2020); (4) Valverde-Vaquero et al. (2007); (5) García Garzón and Locutura (1981); (6) Pereira et al. (2017); (7) Díez Fernández and Pereira et al. (2017); (8) Gutiérrez-Alonso et al. (2015), Díez Fernández and Pereira et al. (2017). (For interpretation of the references to colour in this figure legend, the reader is referred to the web version of this article.)

the Feli granite belongs to the late-D₃, perphosphorus, Ca-poor monzogranitic series. The *Qz-cas* veins, which are located over this hidden pluton, have an age of 300.1 ± 3.1 Ma, which is in the range of that of the Feli granite (Fig. 11). Therefore, the second magmatic event in the FA area would correspond to the intrusion of the Feli pluton followed by the crystallization of the cassiterite-rich quartz veins during a hydrothermal stage.

The third and last magmatic event is the most important in relation to the highly evolved pegmatites from the FA area. This event would be related to the youngest facies of the MEPL that shows intrusive field relationships with respect to the main facies of the MEPL complex, on the Portuguese side, and with $^{206}Pb/^{238}U$ age of 300.0 ± 2.2 Ma (Ferreira et al., 2019). This age is similar to that of the barren *aplitic-pegmatitic apophyses*, directly related to the undeformed East-MEPL facies (Spanish side), with an age of 300.4 ± 3.2 Ma (Figs. 2 and 11). Despite the lack of geochronological data on the Saucelle granite, limiting the FA field to the NE (Fig. 2), it may be included into this third event of late- to post-D₃ Variscan granites based on geological relationships (Dias da Silva, 2014; Silva and Ribeiro, 1994).

The subvertical intermediate and Li-rich pegmatite dikes are the most evolved in the FA field and appear to have also developed during the third magmatic event. Taking into account the difference in the apparent plateau ages (>10 Ma) between these pegmatites and the syn-D₃ facies of the MEPL complex, we can rule out the syn-D₃ Variscan granites as potential sources for these pegmatites. The apparent plateau

ages obtained for the *intermediate* and *spodumene-rich* pegmatites, 304.3 ± 4.0 and 303.6 ± 4.8 Ma respectively, differ approximately 8 Ma from other evolved pegmatites (*petalite-rich, Li-mica + spodumene-rich* and *Li-mica-rich*), with ages in the range 295.1 ± 3.9 to 296.7 ± 3.5 Ma (Figs. 6 and 11, Table 2; Supplementary Tables 1 and 2). However, as already discussed, it is conceivable to assume a cogenetic origin for the intermediate and the four types of Li-rich pegmatites. The high apparent plateau ages obtained for the *intermediate* and *spodumene-rich* pegmatites may be related to the incorporation of non-radiogenic Ar. The obtained plateau spectra are very regular denoting an absence of Ar excess, which could be related to the homogeneous distribution of non-radiogenic Ar in all analysed mica structures (Hanes, 1991). In any case, taking into account the analytical error, all the ages obtained for the intermediate and Li-rich pegmatites belong to the same range, with a mean age value of 299 ± 3.9 Ma, nearly similar to that of 302 ± 3 Ma columbite U—Pb age of a *Li-mica-rich pegmatite* (Fig. 7). Accordingly, it may be assumed that the Li-rich pegmatites from the FA field are related to a non-outcropping, late- to post-D₃ (≈ 295–300 Ma) granite, which could resemble the East-MEPL facies or the Saucelle granite (Fig. 11).

Summing up, the zoning observed nowadays in the FA pegmatitic field (Fig. 2), would respond to the overlap of three main magmatic events during syn- and late- to post-D₃ Variscan orogenic stages (≈320 to 295 Ma), with a more or less continuous magmatic activity along this period.

6. Conclusions

(1) In the FA area 10 pegmatite types may be distinguished, some of them highly fractionated and enriched in Li. According to their degree of fractionation four types of barren pegmatites (*intragranitic, concordant quartz + andalusite-rich layers, concordant barren pegmatites*, and *aplitic-pegmatitic apophyses*); two types of intermediate pegmatites (*K-feldspar-rich and intermediate pegmatites*); and four types of Li-rich evolved pegmatites (*petalite-rich, spodumene-rich, Li-mica + spodumene-rich* and *Li-mica-rich pegmatites*) have been distinguished. In addition, a group of *cassiterite-rich quartz hydrothermal veins* occurs at the north of the FA field.

(2) Magmatic activity in the FA area during syn- and late to post-D_3 stages (i. e. from ≈ 320 to 295 Ma) of the Variscan orogeny was important and nearly continuous, with the overlap of different granitic units. Volumetrically, the most important in outcrop corresponds to the MEPL, which is the oldest one (≈319–311 Ma) and may be included in the two-mica leucogranitic series of highly peraluminous, Ca-poor leucogranites, with a metasedimentary protolith. The other granitic units in the area (East-MEPL, Saucelle and Feli), are younger (≈305–300 Ma), and may be included in the series of perphosphorus, highly peraluminous and Ca-poor monzogranites, also with a metasedimentary source.

(3) Structural, chemical, textural and mineralogical features, field relationships and $^{40}Ar*/^{39}Ar$ isotopic dating reveal a non-cogenetic character for the pegmatites, forming along three periods: (i) (≈ 319-311 Ma) with the syn-D_3 Mêda-Escalhão-Penedono-Lumbrales granitic complex (MEPL) and most barren pegmatites (*intragranitic, concordant quartz + andalusite layers*, and *concordant simple pegmatites*); (ii) (≈305-300 Ma) corresponds to the late- to post-D_3 Feli metasomatized granite and the *cassiterite-rich quartz veins*; and (iii) (≈300-295 Ma) represented by the late- to post-D_3 East-MEPL and Saucelle granites, with possible linkage to the *barren aplitic-pegmatitic apophyses*, and the discordant intermediate and Li-rich pegmatites.

(4) Regional distribution in the pegmatitic field is not the result of a single fractionation trend, but of the juxtaposition of non-cogenetic pegmatites derived from different granitic magmas, mainly by fractional crystallization processes.

(5) The six types of discordant pegmatites (two intermediate and four Li-rich pegmatite types) share textural, structural, mineralogical, geochronological and geochemical features, which allow to include them in the same fractionation trend. Pegmatitic melts derived from P-rich, Ca-poor granitic melts (East-MEPL, Saucelle granite or a non-outcropping equivalent granite).

Supplementary data to this article can be found online at https://doi.org/10.1016/j.lithos.2023.107195.

Author contributions

All authors contributed to the study conception and design. Material preparation, data collection and analysis were performed by E. Roda-Robles, R. Vieira, J. Cardoso-Fernandes, J. Errandonea-Martin and I. Garate-Olave. The first draft of the manuscript was written by E. Roda-Robles and all authors commented on previous versions of the manuscript. All authors read and approved the final manuscript.

Funding

Declaration of Competing Interest

The authors declare no conflict of interest. The funders had no role in the design of the study; in the collection, analyses, or interpretation of data; in the writing of the manuscript, or in the decision to publish the results.

Acknowledgments

References

Antunes, I.M.H.R., Neiva, A.M.R., Silva, M.M.V.G., Corfu, F., 2008. Geochemistry of S type granitic rocks from the reversely zoned Castelo Branco pluton (Central Portugal). Lithos 103, 445–465.

Barbero, L., Villaseca, C., Rogers, G., Brown, P.E., 1995. Geochemical and isotopic disequilibrium in crustal melting: an insight from the anatectic granitoids from Toledo, Spain. J. Geophys. Res. 100, 15745–15765.

Bea, F., Montero, P., Molina, J.F., 1999. Mafic precursors, peraluminous granitoids, and late lamprophyres in the Avila batholith: a model for the generation of Variscan batholiths in Iberia. J. Geol. 107, 399–419.

Bea, F., Montero, P., Zinger, T., 2003. The nature, origin, and thermal influence of the granite source layer of Central Iberia. J. Geol. 111, 579–595.

Breiter, K., Ďurišová, J., Korbelová, Z., Lima, A., Vašinová Galiová, M., Hložková, M., Hložková, M., 2021. Rock textures and mineral zoning – a clue to understanding rare-metal granite evolution: Argemela stock, Central-Eastern Portugal. Lithos 410-411, 106562.

Cameron, E.N., Jahns, R.H., McNair, A.H., Page, L.R., 1949. Internal structure of granitic pegmatites. In: Economic Geology, Monograph, p. 2.

Cardoso-Fernandes, J., Silva, J., Perrotta, M.M., Lima, A., Teodoro, A.C., Ribeiro, M.A., Dias, F., Barrès, O., Cauzid, J., Roda-Robles, E., 2021. Interpretation of the reflectance spectra of lithium (Li) minerals and pegmatites: a case study for mineralogical and lithological identification in the Fregeneda–Almendra Area. Remote Sens. 13, 3688.

Černý, P., 1992. Geochemical and petrogenetic features of mineralization in rare-element granitic pegmatites in the light of current research. Appl. Geochem. 7, 397–416.

Černý, P., Ercit, T.S., 2005. The classification of granitic pegmatites revisited. Can. Mineral. 43, 2005–2026.

Debon, F., Le Fort, P., 1983. A chemical–mineralogical classification of common plutonic rocks and associations. Earth Environ. Sci. Trans. Royal Soc. Edinburgh 73, 135–149.

Dias da Silva, I., 2014. Geología de las zonas Centro Ibérica y Galicia–Trás-os-Montes en la parte oriental del Complejo de Morais, Portugal/España [PhD Thesis]. Instituto Universitario de Geología "Isidro Parga Pondal" - Área de Xeoloxía e Minería do Seminario de Estudos Galegos, 424 pp.

Dias da Silva, I., Gómez-Barreiro, J., Martínez Catalán, J.R., Ayarza, P., Pohl, J., Martínez, E., 2017. Structural and microstructural analysis of the Retortillo Syncline (Variscan belt, Central Iberia). Implications for the Central Iberian Orocline. Tectonophysics 717, 99–115.

Dias, G., Leterrier, J., Mendes, A., Simões, P.P., Bertrand, J.M., 1998. U–Pb zircon and monazite geochronology of post-collisional Hercynian granitoids from the Central Iberian Zone (Northern Portugal). Lithos 45, 349–369.

Díez Fernández, R., Pereira, M.F., 2016. Extensional orogenic collapse captured by strike-slip tectonics: Constraints from structural geology and U-Pb geochronology of the Pinhel shear zone (Variscan orogen, Iberian Massif). Tectonophysics 691, 290–310.

Díez Fernández, R., Pereira, M.F., 2017. Strike-slip shear zones of the Iberian Massif: are they coeval? Lithosphere 5, 726–744.

Errandonea-Martin, J., Sarrionandia, F., Janoušek, V., Carracedo-Sánchez, M., Gil Ibarguchi, J.I., 2019. Origin of cordierite-bearing monzogranites from the southern Central Iberian Zone – Inferences from the zoned Sierra Bermeja Pluton (Extremadura, Spain). Lithos 342–343, 440–462.

Errandonea-Martin, J., Garate-Olave, I., Roda-Robles, E., Cardoso-Fernandes, J., Lima, A., Ribeiro, M.A., Teodoro, A.C., 2022. Metasomatic effect of Li-bearing aplite-pegmatites on psammitic and pelitic metasediments: geochemical constraints on critical raw material exploration at the Fregeneda–Almendra Pegmatite Field (Spain and Portugal). Ore Geol. Rev. 150, 105155 https://doi.org/10.1016/j.oregeorev.2022.105155.

Ferreira, J.A., Bento dos Santos, T., Pereira, I., Mata, J., 2019. Tectonically assisted exhumation and cooling of Variscan granites in an anatectic complex of the Central Iberian Zone, Portugal: constraints from LA - ICP - MS zircon and apatite U–Pb ages. Int. J. Earth Sci. 108, 2153–2175.

Ferreira, J.A., Mata, J., Bento dos Santos, T., Pereira, I., 2020. The role of melting on the geochemical evolution and isotopic variability of an anatectic complex in the Iberian Variscides. Lithos 378–379, 105769.

Fersman, A.E., 1940. Pegmatites. In: Selected Works VI. Granite Pegmatites.Academy of the Sciences of the URSS (Pegmatity. T. 1. Granitnye Pegmatity Rus).

Garate-Olave, I., Roda-Robles, E., Gil-Crespo, P.P., Pesquera, A., Errandonea-Martin, J., 2020. The Tres Arroyos granitic aplite-pegmatite field (Central Iberian Zone, Spain): petrogenetic constraints from evolution of Nb-Ta-Sn oxides, whole-rock geochemistry and U-Pb geochronology. Minerals 10, 1008.

García Garzón, J., Locutura, J., 1981. Datación por el método Rb-Sr de los granitos de Lumbrales-Sobradillo y Villar de Ciervos-Puerto Seguro. Boletín geológico y minero XCII, pp. 68–72.

Gomes, M.E.P., Teixeira, R.J.S., Neiva, A.M.R., Corfu, F., 2014. Geochemistry and geochronology of granitoids from Bemposta-Picote region, Northeastern Portugal. Comun. Geol. 101, 115–118.

González-Menéndez, L., Azor, A., Rubio-Ordóñez, Á., Sánchez-Almazo, I., 2011. The metamorphic aureole of the Nisa-Alburquerque batholith (SW Iberia): implications for deep structure and emplacement mode. Int. J. Earth Sci. 100, 1533–1550.

Gonzalo Corral, J.C., 1981. Estudio geológico del campo filoniano de La Fregeneda (Salamanca) [Tesis de Licenciatura].. Universidad de Salamanca, 77 pp.

Gutiérrez-Alonso, G., Collins, A.S., Fernández-Suárez, J., Pastor-Galán, D., González-Clavijo, E., Jourdan, F., Weil, A., Johnston, S.T., 2015. Dating of lithospheric buckling: ⁴⁰Ar/³⁹Ar ages of syn-orocline strike–slip shear zones in northwestern Iberia. Tectonophysics 643, 44–54.

Hanes, J.A., 1991. K-Ar and ⁴⁰Ar/³⁹Ar geochronology: Methods and applications. In: Heaman, L., Ludden, J.N. (Eds.), Applications of Radiogenic Isotope Systems to Problems in Geology. Mineralogical Association Of Canada Short Course Handbook, 19, pp. 27–57.

Harrison, T., Celerier, J., Aikman, A., Hermann, J., Heizler, M., 2009. Diffusion of 40Ar in muscovite. Geochim. Cosmochim. Acta 73, 1039–1051.

Jahns, R.H., 1953. The genesis of Pegmatites 2. Quantitative analysis of lithium-bearing pegmatite, Mora County, New-Mexico. Am. Mineral. 38, 1078–1112.

Jolliff, B.L., Papike, J.J., Shearer, C.K., 1992. Petrogenetic relationships between pegmatite and granite based on geochemistry of muscovite in pegmatite wall zones, Black Hills, South Dakota, USA. Geochim Cosmochim Acta 56, 1915–1939.

Julivert, M., Marcos, A., Truyols, J., 1972. L'évolution paléogéographique du NW de l'Espagne pendant l'Ordovicien-Silurien. Bulletin de la Société géologique et minéralogique de Bretagne 4, 1–7.

London, D., 2008. Pegmatites. The Canadian Mineralogist, Special Publication n° 10, 417 pp.

London, D., 2018. Ore-forming processes within granitic pegmatites. Ore Geol. Rev. 101, 349–383.

López-Moro, F.J., López-Plaza, M., Romer, R.L., 2012. Generation and emplacement of shear-related highly mobile crustal melts: the synkinematic leucogranites from the Variscan Tormes Dome, Western Spain. Int. J. Earth Sci. 101, 1273–1298.

López-Moro, F.J., López-Plaza, M., Gutiérrez-Alonso, G., Fernández-Suárez, J., López-Carmona, A., Hofmann, M., Romer, R.L., 2018. Crustal melting and recycling: geochronology and sources of Variscan syn-kinematic anatectic granitoids of the Tormes Dome (Central Iberian Zone). A U–Pb LA-ICP-MS study. Int. J. Earth Sci. 107, 985–1004.

López-Plaza, M., Martínez-Catalán, J.R., 1987. Síntesis estructural de los granitoides del Macizo Hespérico. In: Bea, F., Carnicero, A., Gonzalo, J.C., López Plaza, M., Rodríguez Alonso, M.D. (Eds.), Geología de los granitoides y rocas asociadas del Macizo Hespérico. Libro homenaje a García de Figuerola LC, Rueda, Madrid, pp. 195–210.

Mangas, J., Arribas, A., 1988. Evolution of hydrothermal fluids in the Feli tin deposit, western Spain. Bull. Mineral. 3, 343–358.

Martín-Izard, A., Reguilón, R., Palero, F., 1992. Las mineralizaciones litiníferas del oeste de Salamanca y Zamora. Estud. Geol. 48, 9–13.

Martins, F., Azevedo, M.R.R., Valle Aguado, B., Gomes, E.P., Tassinari, C., Neto, J.N., 2020. Shrimp u-pb ages and ree patterns for zircon from an anatectic Variscan two-mica granite from the bemposta migmatite complex (central iberian zone). Can. Mineral. 58, 847–886.

Milord, I., Sawyer, E.W., Brown, M., 2001. Formation of diatexite migmatite and granite magma during anatexis of semi-pelitic metasedimentary rocks: an example from St. Malo, France. J. Petrol. 42, 487–505.

Neiva, A.M.R., Gomes, C.L., Silva, P.B., Gomes, M.E.P., dos Santos, A.C.T., 2019. Geochemistry of granitic aplite-pegmatite dykes and sills and their minerals from the Gravanho-Gouveia area in Central Portugal. Geochemistry 79, 221–234.

Nitschke, S.H., 1999. Tungsten and Fluorine in calc-silicate rocks at Riba de Alva, northeastern Portugal. Chronique de la recherche minière, 535, pp. 3–17.

Norton, J.J., 1973. Lithium, cesium and rubidium - the rare alkali metal: United States mineral resources. U.S. Geol. Surv. Prof. Pap. 820, 365–378.

Novák, M., Kadlec, T., Gadas, P., 2013. Geological position, mineral assemblages and contamination of granitic pegmatites in the Moldanubian Zone, Czech Republic; examples from the Vlastejovice region. J. Geosci. 58, 21–47.

Pereira, I., Dias, R., Bento dos Santos, T., Mata, J., 2017. Exhumation of a migmatite complex along a transpressive shear zone: inferences from the Variscan Juzbado–Penalva do Castelo Shear Zone (Central Iberian Zone). J. Geol. Soc. 174, 1004–1018.

Pereira, M.F., Díez Fernández, R., Gama, C., Hofmann, M., Gärtner, A., Linnemann, U., 2018. S-type granite generation and emplacement during a regional switch from extensional to contractional deformation (Central Iberian Zone, Iberian autochthonous domain, Variscan Orogeny). Int. J. Earth Sci. (Geol Rundsch) 107, 251–267.

Roda, E., Pesquera, A., Velasco, F., 1995a. Tourmaline in granitic pegmatites and their country rocks, Fregeneda Area, Salamanca, Spain. Can. Mineral. 33, 835–848.

Roda, E., Pesquera, A., Velasco, F., 1995b. Micas of the Muscovite-Lepidolite series from the Fregeneda Pegmatites (Salamanca, Spain). Mineral. Petrol. 55, 145–157.

Roda, E., Fontan, F., Pesquera, A., Velasco, F., 1996. The phosphate mineral association of the granitic pegmatites of the Fregeneda area (Salamanca, Spain). Mineral. Mag. 60, 767–778.

Roda-Robles, E., 1993. Distribución, características y petrogénesis de las pegmatitas de La Fregeneda (Salamanca) [PhD Thesis].. Universidad del País Vasco, Spain, 199 pp.

Roda-Robles, E., Pesquera, A., Velasco, F., Fontan, F., 1999. The granitic pegmatites of the Fregeneda area (Salamanca, Spain): characteristics and petrogenesis. Mineral. Mag. 63, 535–558.

Roda-Robles, E., Vieira, R., Lima, A., Pesquera, A., 2009. Petrogenetic links between granites and pegmatites in the Fregeneda-Almendra area (Salamanca, Spain and Guarda, Portugal): new insights from ⁴⁰Ar/³⁹Ar dating in micas. Estud. Geol. 19, 305–310.

Roda-Robles, E., Vieira, R., Pesquera, A., Lima, A., 2010. Chemical variations and significance of phosphates from the Fregeneda-Almendra pegmatite field, Central Iberian Zone (Spain and Portugal). Mineral. Petrol. 100, 23–34.

Roda-Robles, E., Pesquera, A., Gil-Crespo, P., Torres-Ruiz, J., 2012. From granite to highly evolved pegmatite: a case study of the Pinilla de Fermoselle granite–pegmatite system (Zamora, Spain). Lithos 153, 192–207.

Roda-Robles, E., Pesquera, A., Gil-Crespo, P.P., Vieira, R., Lima, A., Garate-Olave, I., Martins, T., Torres-Ruiz, J., 2016. Geology and mineralogy of Li mineralization in the Central Iberian Zone (Spain and Portugal). Mineral. Mag. 80, 103–126.

Roda-Robles, E., Villaseca, C., Pesquera, A., Gil-Crespo, P.P., Vieira, R., Lima, A., Garate-Olave, I., 2018. Petrogenetic relationships between Variscan granitoids and Li-(F-P)-rich aplite-pegmatites in the Central Iberian Zone: geological and geochemical constraints and implications for other regions from the European Variscides. Ore Geol. Rev. 95, 408–430.

Rodríguez Fernández, L.R., Oliveira, J.T., 2015. Mapa geológico de España y Portugal a escala 1:1.000.000. Instituto Geológico y Minero de España. Laboratório Nacional de Energia e Geologia de Portugal.

Rodríguez Fernández, L.R., Díez Montes, A., Escuder, J., Carrasco, R., 2000. Hoja geológica número 448 (Vilvestre). Instituto Geológico y Minero de España (IGME). Mapa Geológico de España a Escala 1:50.000 (2ª serie). Retrieved from. http://info.igme.es/cartografiadigital/geologica/Magna50Hoja.aspx?Id=448.

Rosenberg, C.L., Handy, M.R., 2005. Experimental deformation of partially melted granite revisited: implications for the continental crust. J. Metamorph. Geol. 23 (1), 19–28.

Rubio-Pascual, F.J., Arenas, R., Martínez-Catalán, J.R., Rodríguez-Fernández, L.R., Wijbrans, J.R., 2014. Thickening and exhumation of the Variscan roots in the Iberian Central System: tectonothermal processes and ⁴⁰Ar/³⁹Ar ages. Tectonophysics 587, 207–221.

Rudnick, R.L., Gao, S., 2014. Composition of the continental crust. In: Holland, H.D., Turekian, K.K. (Eds.), Treatise on Geochemistry, 2nd edition Volume 4: The Crust. Elsevier Science, Oxford, pp. 1–51. https://doi.org/10.1016/B978-0-08-095975-7.00301-6.

Sawyer, E.W., 2020. Petrogenesis of secondary diatexites and the melt budget for crustal reworking. J. Petrol. 61 egaa039.

Silva, A.F., Ribeiro, M.L., 1994. Notícia explicativa da folha 15-B. Instituto Geologico e Mineiro, 48 Freixo de Espada à Cinta – da carta Geológica de Portugal na escala 1/50.000.

Simmons, W.B., Webber, K.L., 2008. Pegmatite genesis: state of the art. Eur. J. Mineral. 20, 421–438.

Simmons, W., Falster, A., Webber, K., Roda-Robles, E., 2016. Bulk composition of mt. Mica pegmatite, Maine, USA: implications for the origin of an LCT type pegmatite by anatexis. Can. Mineral. 54, 1053–1070.

Sokolov, Y.M., 1982. Chapter 12 - Precambrian metamorphogenic pegmatites. In: The Development Potential of Precambrian Mineral Deposits. Pergamon, pp. 157–164.

Talavera, C., Montero, P., Martínez Poyatos, D., Williams, I.S., 2012. Ediacaran to Lower Ordovician age for rocks ascribed to the Schist–Graywacke Complex (Iberian Massif, Spain): evidence from detrital zircon SHRIMP U–Pb geochronology. Gondwana Res. 22, 928–942.

Valverde-Vaquero, P., Díez Balda, M.A., Díez Montes, A., Dörr, W., Escuder Viruete, J., González, C., Maluski, H., Rodríguez Fernández, L.R., Rubio, F., Villar, P., 2007. The "hot orogen": Two separate Variscan low-pressure metamorphic events in the Central Iberian Zone. In: Faure, M., Lardeaux, J.-M., Ledru, P., Peschler, A., Schulmann, K. (Eds.), Mechanics of Variscan Orogeny: A Modern View on Orogenic Research. Géologie de la France. Société Géologique de France and Bureau de Recherches Géologiques et Minières, Paris, p. 168.

Vieira, R., 2010. Aplitopegmatitos com elementos raros da região entre Almendra (V. N. de Foz-Côa) e Barca d'Alba (Figueira de Castelo Rodrigo). In: Campo aplitopegmatítico da Fregeneda-Almendra. Universidade do Porto, Portugal [PhD Thesis]. 275 pp.

Vieira, R., Roda-Robles, E., Pesquera, A., Lima, A., 2011. Chemical variation and significance of micas from the Fregeneda-Almendra pegmatitic field (Central-Iberian Zone, Spain and Portugal). Am. Mineral. 96, 637–645.

Villaseca, C., 2011. On the origin of granite types in the Central Iberian Zone: Contribution from integrated U-Pb and Hf isotope studies of zircon. In: VIII Congresso Ibérico de Geoquímica, pp. 271–276.

Villaseca, C., Barbero, L., Rogers, G., 1998a. Crustal origin of Hercynian peraluminous granitic batholiths of Central Spain: petrological, geochemical and isotopic (Sr, Nd) constraints. Lithos 43, 55–79.

Villaseca, C., Barbero, L., Herreros, V., 1998b. A re-examination of the typology of peraluminous granite types in intracontinental orogenic belts. Trans. R. Soc. Edinb. Earth Sci. 89, 113–119.

Villaseca, C., Pérez-Soba, C., Merino, E., Orejana, D., López-García, J.A., Billstrom, K., 2008. Contrasting crustal sources for peraluminous granites of the segmented Montes de Toledo Batholith (Iberian Variscan Belt). J. Geosci. 53, 263–280.

Webber, K.L., Simmons, W.B., Falster, A.U., Foord, E.E., 1999. Cooling rates and crystallization dynamics of shallow level pegmatite-aplite dikes, San Diego County, California. Am. Mineral. 84, 708–717.

Webber, K., Simmons, W.B., Falster, A.U., Hanson, S., 2019. Anatectic pegmatites of the Oxford County Pegmatite Field, Maine, USA. Can. Mineral. 57, 811–815.